Composite Structures 92 (2010) 1793–1812

Contents lists available at ScienceDirect

Composite Structures

journal homepage: www.elsevier.com/locate/compstruct

Coupled thermo-mechanical analysis of one-layered and multilayered plates

S. Brischetto *, E. Carrera

Department of Aeronautics and Space Engineering, Politecnico di Torino, Italy

ARTICLE INFO

Article history:
Available online 2 February 2010

Keywords:
Multilayered plates
Carrera's Unified Formulation
Thermo-mechanical coupling
Assumed temperature profile
Calculated temperature profile

ABSTRACT

The paper considers a fully coupled thermo-mechanical analysis of one-layered and multilayered isotropic and composite plates. In the proposed analysis, the temperature is considered a primary variable as the displacement; it is therefore directly obtained from the model and this feature permits the temperature field to be evaluated through the thickness direction in three different cases: – static analysis with imposed temperature on the external surfaces; – static analysis of structures subjected to a mechanical load, with the possibility of considering the temperature field effects; – a free vibration problem, with the evaluation of the temperature field effects. In the first case, imposing a temperature at the top and bottom of the plate, the static response is given in term of displacements, stresses and temperature field; the proposed method is very promising if compared to a partially coupled thermo-mechanical analysis, where the temperature is only considered as an external load, and the temperature profile must be a priori defined: considering it linear through the thickness direction or calculating it by solving the Fourier heat conduction equation. In the second case, a mechanical load is applied. The fully coupled thermo-mechanical analysis gives smaller displacement values than those obtained with the pure mechanical analysis; the temperature effect is not considered in this latter approach. The third case is the free vibration problem. The fully coupled thermo-mechanical analysis permits the effect of the temperature field to be evaluated: larger frequencies are obtained with respect to the pure mechanical analysis. Carrera's Unified Formulation is applied to obtain several refined models with orders of expansion in the thickness direction, from linear to fourth-order, for displacements and temperature. Both equivalent single layer and layer wise approaches are considered for the multilayered plates. At present, no benchmarks are available within the framework of a fully coupled theory. This work aims to fill this gap.

1. Introduction

Thermoelasticity is a branch of applied mechanics that is concerned with the effects of heat on the deformation and stresses of solid bodies, which are considered to be elastic. It is therefore considered as an extension of the conventional theory of isothermal elasticity to those processes in which deformation and stresses are produced not only by mechanical forces, but also by temperature variations. Thermoelastic processes are not totally reversible: the elastic part may be reversed (the deformations caused by heat are theoretically recoverable through cooling), but the thermal part may not be reversed because of the dissipation of energy that takes place during heat transfer. The effect of the temperature field on the deformation field is not a one-way phenomenon; it is in fact well known that a deformation of the body produces changes in its temperature. These features demonstrate that the mechanical and thermal aspects are coupled and inseparable [1]. Therefore, this coupling considerably complicates the computational aspect of solving actual thermoelastic problems. As suggested in the introduction to Nowinski's book [1], it is possible to say: *"Practically speaking, it is generally possible to discount the coupling and to evaluate the temperature and deformation fields, in this order, separately"*. The thermoelastic problem, where the temperature and deformation fields are discounted, is here defined as a partially coupled thermo-mechanical problem.

Partially coupled thermo-mechanical models are extensively employed in the analysis of typical aeronautical structures, such as one-layered isotropic and multilayered composite plates and shells, where the temperature variations are one of the most important factors for the stress fields that can cause failure of the structures [2–4]. These structures are subject to severe thermal environments, such as high temperatures, high gradients and cyclic changes in temperature. Because of these implications, the effects of both high-temperature and mechanical loadings have to be considered in the design process. An accurate description of local stress fields in the layers becomes mandatory to prevent thermally loaded structure failure mechanisms. Computational models,

* Corresponding author. Address: Department of Aeronautics and Space Engineering, Politecnico di Torino, Corso Duca degli Abruzzi, 24, 10129 Torino, Italy. Tel.: +39 011 564 6869; fax: +39 011 564 6899.
E-mail address: salvatore.brischetto@polito.it (S. Brischetto).

0263-8223/$ - see front matter © 2010 Elsevier Ltd. All rights reserved.
doi:10.1016/j.compstruct.2010.01.020

developed to study the behavior of high-temperature composite plates and shells, make use of partially coupled thermo-mechanical analysis [4]. The temperature is only considered as an external load and the temperature profile must be a priori defined: considering it "a priori" through the thickness direction [5–10] or calculating it by solving the Fourier heat conduction equation [11–15].

Wu and Chen [5] have described displacements and stresses in laminated structures under thermal bending, assuming a linear temperature profile through the thickness direction. In [6], Brischetto and Carrera have used the same linear temperature profile to asses the accuracy of several refined models for the static analysis of multilayered composite shells. A linear temperature profile through the thickness direction has also been considered by Bhaskar et al. [7] and Khare et al. [8] to analyze the deflection of composite laminates and laminated or sandwich shells, respectively. Khdeir [9] has solved the thermoelastic governing equations by assuming a linear or constant temperature profile through the thickness. An interesting method to analyze the thermal stresses in shells is the use of Cosserat surfaces, as done by Birsan [10] for two given temperature fields.

Other models, given in the open literature, calculate the temperature profile through the thickness: sometimes, "a priori" assumption can lead to very large errors. In the case of multilayered anisotropic structures, the temperature profile is never linear, even when the plate or shell is thin: an incorrect temperature profile gives an erroneous thermal load which leads to larger errors, even though the structural model is accurate [11,12]. A finite element shell has been developed by Rolfes et al. [13] to analyze composite structures simultaneously loaded by mechanical and thermal loads; the temperature profile has been presumed linear or quadratic in the thickness direction and then introduced into the Fourier heat conduction equation. The Fourier heat conduction equation has been solved for multilayered composite shells and for functionally graded material plates in [14,15], respectively. The calculated temperature profile gives an appropriate thermal load to correctly investigate the thermal deflection of such structures.

The present work proposes a fully coupled thermoelastic analysis where both temperature and displacement fields are primary variables in the thermo-mechanical governing equations. This fully coupled model permits several problems, which are of particular interest in the aeronautics and space fields, but not only, to be analyzed, in a very efficient and simple way. Therefore, the case of structures with imposed temperature on the external surfaces is easily solved without the need to a priori define the temperature profile in the thickness direction. The temperature is a primary variable of the problem, and the values of temperature at the top and bottom are directly imposed: the fully coupled thermo-mechanical governing equations directly give the displacements and the temperature through the thickness direction. In order to calculate the displacements, the partially coupled governing equations instead need an a priori temperature profile in the thickness direction (assumed [5–10] or calculated [11–15]) to define the thermal load. The other two possible applications of the fully-coupled governing equations are: an external applied mechanical load and the free vibration problem. These two cases are also investigated in this paper, but a relevant simplification is made: the variation in time of the temperature is not considered, and this means that these two problems are investigated at equilibrium conditions. This great simplification will be removed in a future work in order to investigate the evolution in time of temperature, strain and stress in such problems.

In the open literature, a small amount of work has been devoted to the coupled thermo-mechanical analysis of structures (both thermoelastic and thermoplastic analysis), and only few of them give numerical results. Altay and Dökmeci [16] have described the physical behavior of thermoelastic continuum by means of opportune variational principles. The stress equations of motion and the equation of heat conduction have been written as divergence equations. The strain-mechanical displacement relations and Fourier's heat conduction law have been written as gradient equations. The same authors have extended this method to thermopiezoelectric mediums in [17] by simply adding the charge equation of electrostatics in the divergence equations and the electric field-electric potential relations in the gradient equations. Das et al. [18] have avoided the use of the thermoelastic potential to solve the general problem of one-dimensional linearized simultaneous equations of thermoelasticity. Displacement and thermal fields have been obtained in the Laplace transformation domain. This method could be very useful in thermoelasticity or other coupled fields.

Some papers have investigated the thermo-mechanical coupling when a temperature is applied to the structure. Cannarozzi and Ubertini [19] have proposed a variational method for linear coupled quasi-static thermoelastic analysis. The variational support is a statement in terms of displacement, temperature, stress and heat flux. The statement has been based on the hybrid stress formulation for the elastic part and on the mixed flux-temperature formulation for the thermal part, and it has included the rate dependent terms of the energy balance equations and the initial conditions. Thermal balance and initial conditions have been weakly enforced using temperature as a Lagrange multiplier, and the thermoelastic dissipation term has been expressed via the constitutive equations, in terms of stress and temperature rates. The local displacement, temperature, stress and heat flux errors have been measured in time when temperature and/or displacement have been applied. Comparisons between coupled and uncoupled analysis, and the accuracy and efficiency of the coupled theory have been demonstrated in [20]. A higher-order zig-zag plate theory (for an exhaustive overview on zig-zag models see [21]) has been developed to refine the prediction of the fully coupled mechanical, thermal, and electric behavior. Both in-plane displacement and temperature fields, through the thickness have been constructed by superimposing a linear zig-zag field on to the smooth, globally cubic varying field. The given theory is suitable for the predictions of fully coupled behavior of thick, smart composite plates under combined mechanical, thermal, and electric loads. The same authors have extended the proposed analysis to a three-node triangular finite element in [22]. Ibrahimbegovic et al. [23] have presented a thermo-mechanical coupling model for folded plates or non-smooth shells which can be used for the analysis of the fire-resistance of cellular structures. Thermo-mechanical coupling has been considered, including radiative exchanges and an operator split solution procedure with different time steps. The motivation for the work was the development of predictive models that would be capable of describing the inelastic behavior of cellular structures, build either of folded plates and/or non-smooth shells, under sustained long term high-temperature effects. In [24], Lee has fully discussed the thermoelasticity problem of multilayered adiabatic and clamped hollow cylinders whose boundaries are subjected to time-dependent temperatures. Solutions for the temperature, displacement and thermal stress distributions have been obtained in both a transient and steady state. The method has developed stable solutions at a specific time. Tanaka et al. [25] have proposed a new boundary element method for the analysis of quasi-static problems in coupled thermoelasticity. Through some mathematical manipulations of the Navier equation in elasticity, the heat conduction equation has been transformed into a simpler form, similar to the uncoupled-type equation with the modified thermal conductivity which shows the coupling effects. This procedure has made it possible to treat the coupled thermoelastic problem as an uncoupled one.

The effect of thermo-mechanical coupling in structures, subjected to mechanical loads, has been investigated by Carrera et al. [26]. A fully coupled thermoelastic analysis of a homogeneous isotropic plate, with a thickness ratio of $a/h = 10$, has been developed. When a mechanical load is applied, a small part of the work done by this load is used to develop an increment in temperature (the maximum value is 0.002 K). The value is remarkably small because of the small coupling effect between the thermal and mechanical field. By discarding the thermal field, a pure mechanical model gives a larger displacement than the displacement obtained with a fully coupled model (the difference is less than 1%, as suggested in Nowinski's book [1]). Daneshjoo and Ramezani [27,28] have proposed a new mixed finite element formulation to analyze transient coupled thermoelastic problems. Two simply supported plates, subjected to half-sine mechanical and thermal loads, have been considered. When a mechanical load is applied, the differences between the coupled and uncoupled analysis are minimum, in terms of stresses. A variational formulation of the coupled thermo-mechanical analysis of dissipative solids has been given in [29], where the boundary-value problem is presented. The problem has considered the equilibrium case for a deformable, inelastic and dissipative solid with the heat conduction problem appended in addition. The equilibrium and external temperature have been considered equal at equilibrium; the variational framework predicts the fraction of dissipated energy (plastic work) that has been converted into heat. Adam and Ponthot [30] have described an updated Enhanced Assumed Strain (EAS) finite element formalism developed to model the thermo-mechanical behavior of metals submitted to large strains. Applications involving finite strains and important thermo-mechanical couplings have been studied. Comparisons between a thermo-mechanical and an isothermal mechanical model have been investigated.

Dynamic thermo-mechanical analysis has been summarized in the following papers. Altay and Dökmeci [31] have considered the thermal relaxation term in the dissipation function. A three-dimensional theory of coupled thermoelasticity has been given for a shell geometry. High-frequency vibrations of temperature-dependent materials have been investigated. The dynamic response of a thermally loaded elastic structure has been considered in [32]. The thermoelastic coupling term in a heat equation acts like a thermal source that is proportional to the strain rate. The thermoelastic coupling effect on the temperature and displacement fields has been measured as a function of the normalized frequency. It has been concluded that the inclusion of dynamic thermoelastic coupling effects in the analysis of space structures should be considered whenever the applied thermal load contains a significant Fourier component with a frequency that is close to the critical frequency of the structure. Wilms and Cohen [33] have studied wave propagation in a thermoelastically coupled half space. Strain, temperature, stress and particle velocity have been obtained. The dynamic interaction of magneto-thermo-elastic waves has been investigated by Wauer [34]. The thermally induced small thickness vibrations are of particular interest. The displacement and incremental temperature are coupled and the thermoelastic modes have been given. Considering a thermo-mechanical coupling, the obtained results demonstrate that, even though no mechanical damping has been considered, the eigenvalues have been characterized by their imaginary part (natural frequency) and also by their non vanishing (negative) real part (dissipation). A modified model of thermoelasticity, with an extra thermal stress effect and wave-type heat conduction, has been given by Kosinski and Frischmuth [35]. The model has been governed by a system of quasi-linear hyperbolic equations. All the essential material functions have been examined, and the impact of their nonlinearity on the solution of initial-boundary-value problems has been studied. However, already at this temperature, the model solutions do not differ numerically from solutions obtained on the basis of Fourier's heat conduction law. This is not true around the critical temperature, where the error reaches about 1000% of the Fourier result. Thermoelastic vibrations of a free supported and clamped circular plate caused by a thermal shock on the surface have been analyzed in [36]. The partial differential equations of the coupled system has been reduced to Volterra's first and second kind of integral equations in the time domain. Very rapid thermal processes, under the action of a thermal shock (caused, e.g., by a momentary ignition and combustion in the rocket engine chamber) are interesting from the thermoelasticity point of view, since they require an analysis of the coupled temperature and deformation fields. This means that the temperature shock induces very rapid movements in the structure elements, thus causing the rise of very significant inertial forces, and, thereby, a rise in vibrations. Rapidly changeable contractions and the expansions in oscillatory movements generate temperature changes in the material which is susceptible to diffusion due to the heat conduction. This means that, in the case of the exact solution, the plate behaves as being less rigid. Yeh [37] has presented an analysis of large amplitude thermo-mechanically coupled vibration of a simply supported orthotropic rectangular thin plate. The governing partial differential equation of the large deflection orthotropic rectangular thin plate of thermo-mechanical coupling has been derived and simplified to a set of three non-linear ordinary differential equations using the Galerkin method.

In the fully coupled thermo-mechanical analysis proposed in this work, displacement and temperature fields are approximated in the thickness direction by several refined two-dimensional theories based on Carrera's Unified Formulation [38,39]. A preliminary analysis, for only the coupled free vibration problem, has been proposed in [40]. In the case of multilayered plates, both equivalent single layer (ESL) and layer wise (LW) approaches have been developed, as suggested in Section 2. The geometrical relations of the plates, in the case of small deformations, are those given in Section 3. Constitutive equations, for the coupled thermo-mechanical analysis, have been obtained from thermoelastic enthalpy density, written in a quadratic form for a linear interaction, see Section 4. The principle of virtual displacements (PVD) can be extended to both partially and fully coupled thermo-mechanical analysis, as done in Section 5. The multilayered plates are considered simply supported with harmonic loads, therefore closed-form solutions are obtained in Navier form, as discussed in Section 6. The results, concerning the applied temperature case, the imposed mechanical load and the free vibration problem, are given in Section 7. The main conclusions are highlighted in Section 8.

2. Carrera's Unified Formulation, CUF

Carrera's Unified Formulation (CUF) is a technique which handles, in a unified manner, a large variety of plate theories [38,39]. According to CUF, the governing equations are written in terms of a few fundamental nuclei which do not formally depend on the order of expansion N used in the thickness direction and on the description of variables (equivalent single layer (ESL) or layer wise (LW)). The application of a two-dimensional method for plates permits the unknown variables to be expressed as a set of thickness functions that only depend on the thickness coordinate z and the correspondent variable which depends on the in-plane coordinates x and y. Therefore, the generic variable $\boldsymbol{f}(x,y,z)$, for instance a displacement, and its variation $\delta\boldsymbol{f}(x,y,z)$ are written according to the following general expansion:

$$\boldsymbol{f}(x,y,z) = F_\tau(z)\boldsymbol{f}_\tau(x,y), \quad \delta\boldsymbol{f}(x,y,z) = F_s(z)\delta\boldsymbol{f}_s(x,y), \quad \text{with} \quad \tau,s = 1,\ldots,N, \tag{1}$$

where the bold letters denote arrays, (x,y) are the in-plane coordinates and z the thickness one. The summing convention, with repeated indexes τ and s, is assumed. The order of expansion N goes from first to fourth-order, and depending on the used thickness functions, a model can be: ESL, when the variable is assumed for the whole multilayer and a Taylor expansion is employed as the thickness functions $F(z)$; LW, when the variable is considered independent in each layer and a combination of Legendre polynomials are used as the thickness functions $F(z)$. In the thermo-mechanical models, proposed in this work, displacements can be modelled in both ESL or LW form, temperature is always considered in LW form. Therefore, a two-dimensional thermo-mechanical model is defined as ESL or LW, depending on the choice made for the displacement vector.

2.1. Equivalent single layer approach

The displacement $\boldsymbol{u} = (u, v, w)$ is described according to equivalent single layer (ESL) description if the unknowns are the same for the whole plate [41] (see Fig. 1). The z expansion is obtained via Taylor polynomials, that is:

$$\begin{aligned} u &= F_0 u_0 + F_1 u_1 + \cdots + F_N u_N = F_\tau u_\tau, \\ v &= F_0 v_0 + F_1 v_1 + \cdots + F_N v_N = F_\tau v_\tau, \\ w &= F_0 w_0 + F_1 w_1 + \cdots + F_N w_N = F_\tau w_\tau, \end{aligned} \tag{2}$$

with $\tau = 0, 1, \ldots, N$; N is the order of expansion that ranges from 1 (linear) to 4:

$$F_0 = z^0 = 1, \quad F_1 = z^1 = z, \quad \ldots, \quad F_N = z^N. \tag{3}$$

Eq. (2) can be written in a vectorial form:

$$\begin{aligned} &\boldsymbol{u}(x,y,z) = F_\tau(z)\boldsymbol{u}_\tau(x,y), \quad \delta\boldsymbol{u}(x,y,z) = F_s(z)\delta\boldsymbol{u}_s(x,y), \\ &\text{with} \qquad \tau, s = 1, \ldots, N. \end{aligned} \tag{4}$$

Simpler theories, such those which discard the ϵ_{zz} effect, can be obtained from refined ESL models: it is sufficient to impose that the transverse displacement w is constant in z. First order Shear Deformation Theory (FSDT) [42] is obtained from an ESL model with linear expansion in the thickness direction z, by imposing a constant transverse displacement w in z. Classical Lamination Theory (CLT) [43–45] is obtained from FSDT via an opportune penalty technique which imposes an infinite transverse shear rigidity. All the ESL theories, with constant or linear transverse displacement w, which means zero or constant transverse normal strain ϵ_{zz}, show Poisson's locking phenomena; this can be overcome via plane stress conditions in constitutive equations [46,47].

2.2. Layer wise approach

When each layer of a multilayered structure is described as independent plates [41], a layer wise (LW) approach is accounted for. The displacement $\boldsymbol{u}^k = (u, v, w)^k$ is described for each layer k, in this way the zigzag form of displacement, in multilayered transverse-anisotropy structures, is easily obtained, as indicated in Fig. 1. The z expansion for displacement components is made for each layer k:

$$\begin{aligned} u^k &= F_0 u_0^k + F_1 u_1^k + \cdots + F_N u_N^k = F_\tau u_\tau^k, \\ v^k &= F_0 v_0^k + F_1 v_1^k + \cdots + F_N v_N^k = F_\tau v_\tau^k, \\ w^k &= F_0 w_0^k + F_1 w_1^k + \cdots + F_N w_N^k = F_\tau w_\tau^k, \end{aligned} \tag{5}$$

with $\tau = 0, 1, \ldots, N$, N is the order of expansion that ranges from 1 (linear) to 4. $k = 1, \ldots, N_l$, where N_l indicates the number of layers. The Eq. (5) written in a vectorial form is:

$$\begin{aligned} &\boldsymbol{u}^k(x,y,z) = F_\tau(z)\boldsymbol{u}_\tau^k(x,y), \quad \delta\boldsymbol{u}^k(x,y,z) = F_s(z)\delta\boldsymbol{u}_s^k(x,y), \\ &\text{with} \qquad \tau, s = t, b, r \quad \text{and} \quad k = 1, \ldots, N_l, \end{aligned} \tag{6}$$

where t and b indicate the top and bottom of each layer k, respectively; r indicates the higher orders of expansion in the thickness direction: $r = 2, \ldots, N$. The thickness functions $F_\tau(\zeta_k)$ and $F_s(\zeta_k)$ have now been defined at the k-layer level, they are a linear combination of Legendre polynomials $P_j = P_j(\zeta_k)$ of the jth-order defined in ζ_k-domain ($\zeta_k = \frac{2z_k}{h_k}$ with z_k local coordinate and h_k thickness, both referred to kth layer, so $-1 \leqslant \zeta_k \leqslant 1$). The first five Legendre polynomials are:

$$\begin{aligned} &P_0 = 1, \quad P_1 = \zeta_k, \quad P_2 = \frac{(3\zeta_k^2 - 1)}{2}, \quad P_3 = \frac{5\zeta_k^3}{2} - \frac{3\zeta_k}{2}, \\ &P_4 = \frac{35\zeta_k^4}{8} - \frac{15\zeta_k^2}{4} + \frac{3}{8}, \end{aligned} \tag{7}$$

their combinations for the thickness functions are:

$$\begin{aligned} &F_t = F_0 = \frac{P_0 + P_1}{2}, \quad F_b = F_1 = \frac{P_0 - P_1}{2}, \quad F_r = P_r - P_{r-2} \\ &\text{with} \qquad r = 2, \ldots, N. \end{aligned} \tag{8}$$

The chosen functions have the following interesting properties:

$$\zeta_k = 1 : F_t = 1; \quad F_b = 0; \quad F_r = 0 \quad \text{at top}, \tag{9}$$

$$\zeta_k = -1 : F_t = 0; \quad F_b = 1; \quad F_r = 0 \quad \text{at bottom}, \tag{10}$$

that is interface values of the variables are considered as variable unknowns, see Fig. 1. This feature permits to easily impose the compatibility conditions for displacements at each layer interface. In LW models, even if a linear expansion in z is considered for transverse displacement w, Poisson's locking phenomena does not appear: the transverse normal strain ϵ_{zz} is piece-wise constant in the thickness direction [46,47].

In case of thermo-mechanical problems, the primary variables are the displacement vector $\boldsymbol{u} = (u, v, w)$ and the scalar sovra-temperature θ (temperature T_1 referred to the reference external room temperature T_0, $\theta = T_1 - T_0$). By considering the higher spatial gradient of the temperature field, the variable θ^k is always modelled as LW [26]:

$$\begin{aligned} &\theta^k(x,y,z) = F_\tau(z)\theta_\tau^k(x,y), \quad \delta\theta^k(x,y,z) = F_s(z)\delta\theta_s^k(x,y), \\ &\text{with} \qquad \tau, s = t, b, r \quad \text{and} \quad k = 1, \ldots, N_l, \end{aligned} \tag{11}$$

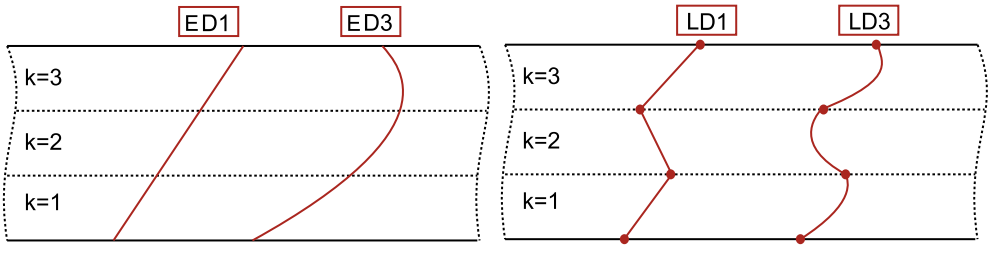

Fig. 1. Equivalent single layer (ESL) vs. layer wise (LW) theories for a multilayered plate.

where t and b indicate the top and bottom of each layer k, respectively. r indicates the higher orders of expansion in the thickness direction: $r = 2, \ldots, N$. The thickness functions are a combination of Legendre polynomials as indicated in Eqs. (7) and (8). The sovra-temperature θ can be considered as an external load [6,14] or as a primary variable [26]. A two-dimensional model for thermo-mechanical problems is defined as ESL or LW depending on the choice made for the displacement vector: the temperature is always considered in LW form.

3. Geometrical relations

We define a thin plate as a three-dimensional body bounded by two closely spaced surfaces, the distance between the two surfaces must be small in comparison with the other dimensions. The middle surface of the plate is the locus of points which lie midway between these surfaces. The distance between the surfaces measured along the normal to the middle surface is the thickness of the plate at that point [48]. The reference system is a rectilinear cartesian one, indicated as (x,y,z) [41]. The in-plane dimensions are indicated with a and b in x and y directions, respectively. The thickness value in z direction is indicated with h. Details can be found in Fig. 2. The geometrical relations for plates, in case of thermo-mechanical problems, link the mechanical strains with the displacement vector and the spatial gradient of temperature with the scalar temperature. The relations split in in-plane (p) and out-of-plane (n) components are:

$$\boldsymbol{\epsilon}^k_{pG} = [\epsilon_{xx}, \epsilon_{yy}, \gamma_{xy}]^{kT} = \boldsymbol{D}_p \boldsymbol{u}^k, \tag{12}$$

$$\boldsymbol{\epsilon}^k_{nG} = [\gamma_{xz}, \gamma_{yz}, \epsilon_{zz}]^{kT} = (\boldsymbol{D}_{np} + \boldsymbol{D}_{nz}) \boldsymbol{u}^k, \tag{13}$$

$$\boldsymbol{\vartheta}^k_{pG} = [\vartheta_x, \vartheta_y]^{kT} = -\boldsymbol{D}_{tp} \theta^k, \tag{14}$$

$$\boldsymbol{\vartheta}^k_{nG} = [\vartheta_z]^k = -\boldsymbol{D}_{tn} \theta^k. \tag{15}$$

$\boldsymbol{\epsilon}^k_{pG}$ and $\boldsymbol{\epsilon}^k_{nG}$ are the in-plane and transverse strains, respectively. $\boldsymbol{u}^k = (u, v, w)^k$ is the displacement vector. $\boldsymbol{\vartheta}^k_{pG}$ and $\boldsymbol{\vartheta}^k_{nG}$ are in-plane and transverse spatial gradients of temperature, respectively. θ^k is the scalar temperature referred to the reference external room temperature. T means the transpose of a vector. The differential operators does not depend on the layer k:

$$\boldsymbol{D}_p = \begin{bmatrix} \partial_x & 0 & 0 \\ 0 & \partial_y & 0 \\ \partial_y & \partial_x & 0 \end{bmatrix}, \quad \boldsymbol{D}_{np} = \begin{bmatrix} 0 & 0 & \partial_x \\ 0 & 0 & \partial_y \\ 0 & 0 & 0 \end{bmatrix}, \quad \boldsymbol{D}_{nz} = \begin{bmatrix} \partial_z & 0 & 0 \\ 0 & \partial_z & 0 \\ 0 & 0 & \partial_z \end{bmatrix},$$

$$\boldsymbol{D}_{tp} = \begin{bmatrix} \partial_x \\ \partial_y \end{bmatrix}, \quad \boldsymbol{D}_{tn} = [\partial_z]. \tag{16}$$

The symbols in differential operators matrices indicate the partial derivatives $\partial_x = \frac{\partial}{\partial x}$, $\partial_y = \frac{\partial}{\partial y}$ and $\partial_z = \frac{\partial}{\partial z}$. Further details for geometrical relations of plates, in case of thermo-mechanical problems, can be found in [26].

$$p_z(x,y) = p_{zt} \sin\left(\frac{m\pi}{a} x\right) \sin\left(\frac{n\pi}{b} y\right)$$

or

$$\theta(x,y) = \theta_t \sin\left(\frac{m\pi}{a} x\right) \sin\left(\frac{n\pi}{b} y\right)$$

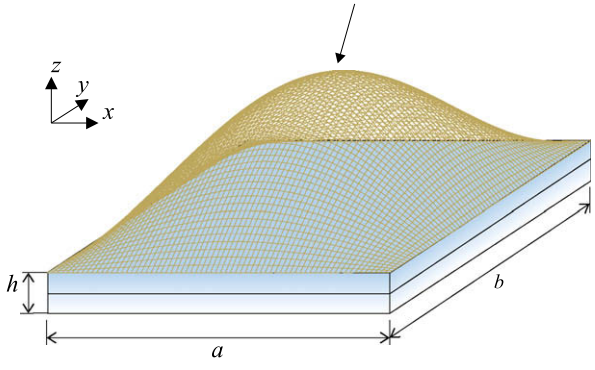

Fig. 2. Reference system for a multilayered plate. Mechanical load or sovra-temperature applied on the top surface.

4. Constitutive equations

Constitutive equations, for the thermo-mechanical problem, are obtained in accordance with that reported in [26,49]. The coupling between the mechanical and thermal fields can be determined by using thermodynamical principles and Maxwell's relations [16,17,19,31]. For this aim, it is necessary to define a *Gibbs free-energy function* G and a *thermomechanical enthalpy density* H [1,50]:

$$G(\epsilon_{ij}, \theta) = \sigma_{ij}\epsilon_{ij} - \eta\theta, \tag{17}$$

$$H(\epsilon_{ij}, \theta, \vartheta_i) = G(\epsilon_{ij}, \theta) - F(\vartheta_i), \tag{18}$$

where σ_{ij} and ϵ_{ij} are the stress and strain components. η is the variation of entropy per unit of volume, and θ the temperature considered with respect to the reference temperature T_0. The function $F(\vartheta_i)$ is the dissipation function, it depends by the spatial temperature gradient ϑ_i:

$$F(\vartheta_i) = \frac{1}{2}\kappa_{ij}\vartheta_i\vartheta_j - \tau_0\dot{h}_i, \tag{19}$$

where κ_{ij} is the symmetric, positive semidefinite conductivity tensor. In the second term, τ_0 is a thermal relaxation parameter and $\dot{h}_i$ is the temporal derivative of the heat flux h_i. The thermal relaxation parameter is omitted in the present work. Further details about the dissipation function $F(\vartheta_i)$ can be found in [16,19,29].

The thermomechanical enthalpy density H can be expanded in order to obtain a quadratic form for a linear interaction:

$$H(\epsilon_{ij}, \theta, \vartheta_i) = \frac{1}{2}Q_{ijkl}\epsilon_{ij}\epsilon_{kl} - \lambda_{ij}\epsilon_{ij}\theta - \frac{1}{2}\chi\theta^2 - \frac{1}{2}\kappa_{ij}\vartheta_i\vartheta_j, \tag{20}$$

where Q_{ijkl} is the elastic coefficients tensor considered for an orthotropic material in the problem reference system [41]. λ_{ij} are the thermo-mechanical coupling coefficients, $\chi = \frac{\rho C_v}{T_0}$ where ρ is the material density, C_v is the specific heat per unit mass and T_0 is the reference temperature [26].

The constitutive equations are obtained by considering the following relations:

$$\sigma_{ij} = \frac{\partial H}{\partial \epsilon_{ij}}, \quad \eta = -\frac{\partial H}{\partial \theta}, \quad h_i = -\frac{\partial H}{\partial \vartheta_i}. \tag{21}$$

By considering Eqs. (20) and (21), we can obtain the constitutive equations for the thermo-mechanical problem:

$$\sigma_{ij} = Q_{ijkl}\epsilon_{kl} - \lambda_{ij}\theta, \tag{22}$$

$$\eta = \lambda_{ij}\epsilon_{ij} + \chi\theta, \tag{23}$$

$$h_i = \kappa_{ij}\vartheta_j. \tag{24}$$

Above equations can be written in single-subscript notation by using the indexes $m = q = 1, 2, 3, 4, 5, 6$ and $i = j = 1, 2, 3$:

$$\sigma_m = Q_{mq}\epsilon_q - \lambda_m\theta, \tag{25}$$

$$\eta = \lambda_q\epsilon_q + \chi\theta, \tag{26}$$

$$h_i = \kappa_{ij}\vartheta_j. \tag{27}$$

From the equations written in single-subscript notations, it is easy to write their matrix form; the matrices and vectors are indicated in bold scripture. Considering a generic multilayered structure, Eqs. (25)–(27) are written for a generic layer k in the problem reference system (x, y, z) as:

$$\boldsymbol{\sigma}^k = \mathbf{Q}^k \boldsymbol{\epsilon}^k - \boldsymbol{\lambda}^k \theta^k, \tag{28}$$

$$\eta^k = \boldsymbol{\lambda}^{kT} \boldsymbol{\epsilon}^k + \chi^k \theta^k, \tag{29}$$

$$\boldsymbol{h}^k = \boldsymbol{\kappa}^k \boldsymbol{\vartheta}^k, \tag{30}$$

where the sovra-temperature θ^k, the term χ^k and the entropy for unite volume η^k are scalar variables in each layer k. The (6×1) vectors of stress and strain components are:

$$\boldsymbol{\sigma}^k = \begin{Bmatrix} \sigma_{xx} \\ \sigma_{yy} \\ \sigma_{zz} \\ \sigma_{yz} \\ \sigma_{xz} \\ \sigma_{xy} \end{Bmatrix}^k, \quad \boldsymbol{\epsilon}^k = \begin{Bmatrix} \epsilon_{xx} \\ \epsilon_{yy} \\ \epsilon_{zz} \\ \gamma_{yz} \\ \gamma_{xz} \\ \gamma_{xy} \end{Bmatrix}^k. \tag{31}$$

The (3×1) vectors of heat flux $\boldsymbol{h}^k$ and spatial gradient of temperature $\boldsymbol{\vartheta}^k$ are:

$$\boldsymbol{h}^k = \begin{Bmatrix} h_x \\ h_y \\ h_z \end{Bmatrix}^k, \quad \boldsymbol{\vartheta}^k = \begin{Bmatrix} \vartheta_x \\ \vartheta_y \\ \vartheta_z \end{Bmatrix}^k. \tag{32}$$

The (6×1) array of thermo-mechanical coupling coefficients $\boldsymbol{\lambda}^k$ is:

$$\boldsymbol{\lambda}^k = \mathbf{Q}^k \boldsymbol{\alpha}^k = \begin{Bmatrix} \lambda_1 \\ \lambda_2 \\ \lambda_3 \\ 0 \\ 0 \\ \lambda_6 \end{Bmatrix}^k, \tag{33}$$

where the elastic coefficients matrix $\mathbf{Q}^k$ of Hooke law, in problem reference system for an orthotropic material [41], is:

$$\mathbf{Q}^k = \begin{bmatrix} Q_{11} & Q_{12} & Q_{13} & 0 & 0 & Q_{16} \\ Q_{12} & Q_{22} & Q_{23} & 0 & 0 & Q_{26} \\ Q_{13} & Q_{23} & Q_{33} & 0 & 0 & Q_{36} \\ 0 & 0 & 0 & Q_{44} & Q_{45} & 0 \\ 0 & 0 & 0 & Q_{45} & Q_{55} & 0 \\ Q_{16} & Q_{26} & Q_{36} & 0 & 0 & Q_{66} \end{bmatrix}^k, \tag{34}$$

the vector $\boldsymbol{\alpha}^k$ has dimension (6×1) and contains the thermal expansion coefficients:

$$\boldsymbol{\alpha}^k = \begin{Bmatrix} \alpha_1 \\ \alpha_2 \\ \alpha_3 \\ 0 \\ 0 \\ 0 \end{Bmatrix}^k. \tag{35}$$

The matrix $\boldsymbol{\kappa}^k$ of conductivity coefficients has dimension (3×3):

$$\boldsymbol{\kappa}^k = \begin{bmatrix} \kappa_{11} & \kappa_{12} & 0 \\ \kappa_{12} & \kappa_{22} & 0 \\ 0 & 0 & \kappa_{33} \end{bmatrix}^k. \tag{36}$$

In order to use the relations proposed in Eqs. (28)–(30) in the proposed variational statement, that will be presented in the next section, it is convenient to split them in in-plane components (subscript p) and out-of-plane components (subscript n). Other two new subscripts are introduced: the subscript C for those variables, in the variational statements, which need the substitution of constitutive equations; the subscript G for those variables, in constitutive equations, which need the substitution of geometrical relations (see Section 3). The split stress and strain components vectors are:

$$\boldsymbol{\sigma}^k_{pC} = \begin{Bmatrix} \sigma_{xx} \\ \sigma_{yy} \\ \sigma_{xy} \end{Bmatrix}^k, \quad \boldsymbol{\sigma}^k_{nC} = \begin{Bmatrix} \sigma_{xz} \\ \sigma_{yz} \\ \sigma_{zz} \end{Bmatrix}^k, \quad \boldsymbol{\epsilon}^k_{pG} = \begin{Bmatrix} \epsilon_{xx} \\ \epsilon_{yy} \\ \gamma_{xy} \end{Bmatrix}^k, \quad \boldsymbol{\epsilon}^k_{nG} = \begin{Bmatrix} \gamma_{xz} \\ \gamma_{yz} \\ \epsilon_{zz} \end{Bmatrix}^k. \tag{37}$$

The vectors (3×1) of heat flux and spatial gradient of the temperature, split in in-plane and out-of-plane components, are:

$$\boldsymbol{h}^k_{pC} = \begin{Bmatrix} h_x \\ h_y \end{Bmatrix}^k, \quad \boldsymbol{h}^k_{nC} = \{ h_z \}^k, \quad \boldsymbol{\vartheta}^k_{pG} = \begin{Bmatrix} \vartheta_x \\ \vartheta_y \end{Bmatrix}^k, \quad \boldsymbol{\vartheta}^k_{nG} = \{ \vartheta_z \}^k. \tag{38}$$

By considering Eqs. (37) and (38), the split form of Eqs. (28)–(30) is:

$$\boldsymbol{\sigma}^k_{pC} = \mathbf{Q}^k_{pp} \boldsymbol{\epsilon}^k_{pG} + \mathbf{Q}^k_{pn} \boldsymbol{\epsilon}^k_{nG} - \boldsymbol{\lambda}^k_p \theta^k, \tag{39}$$

$$\boldsymbol{\sigma}^k_{nC} = \mathbf{Q}^k_{np} \boldsymbol{\epsilon}^k_{pG} + \mathbf{Q}^k_{nn} \boldsymbol{\epsilon}^k_{nG} - \boldsymbol{\lambda}^k_n \theta^k, \tag{40}$$

$$\eta^k_C = \boldsymbol{\lambda}^{kT}_p \boldsymbol{\epsilon}^k_{pG} + \boldsymbol{\lambda}^{kT}_n \boldsymbol{\epsilon}^k_{nG} + \chi^k \theta^k, \tag{41}$$

$$\boldsymbol{h}^k_p = \boldsymbol{\kappa}^k_{pp} \boldsymbol{\vartheta}^k_{pG} + \boldsymbol{\kappa}^k_{pn} \boldsymbol{\vartheta}^k_{nG}, \tag{42}$$

$$\boldsymbol{h}^k_n = \boldsymbol{\kappa}^k_{np} \boldsymbol{\vartheta}^k_{pG} + \boldsymbol{\kappa}^k_{nn} \boldsymbol{\vartheta}^k_{nG}. \tag{43}$$

The explicit forms of the split matrices in Eqs. (39)–(43) are:

- Elastic coefficients matrices:

$$\mathbf{Q}^k_{pp} = \begin{bmatrix} Q_{11} & Q_{12} & Q_{16} \\ Q_{12} & Q_{22} & Q_{26} \\ Q_{16} & Q_{26} & Q_{66} \end{bmatrix}^k, \quad \mathbf{Q}^k_{pn} = \begin{bmatrix} 0 & 0 & Q_{13} \\ 0 & 0 & Q_{23} \\ 0 & 0 & Q_{36} \end{bmatrix}^k,$$

$$\mathbf{Q}^k_{np} = \begin{bmatrix} 0 & 0 & 0 \\ 0 & 0 & 0 \\ Q_{13} & Q_{23} & Q_{36} \end{bmatrix}^k, \quad \mathbf{Q}^k_{nn} = \begin{bmatrix} Q_{55} & Q_{45} & 0 \\ Q_{45} & Q_{44} & 0 \\ 0 & 0 & Q_{33} \end{bmatrix}^k. \tag{44}$$

- Thermo-mechanical coupling coefficients:

$$\boldsymbol{\lambda}^k_p = \begin{bmatrix} \lambda_1 \\ \lambda_2 \\ \lambda_6 \end{bmatrix}^k, \quad \boldsymbol{\lambda}^k_n = \begin{bmatrix} 0 \\ 0 \\ \lambda_3 \end{bmatrix}^k. \tag{45}$$

- Conductivity coefficients:

$$\boldsymbol{\kappa}^k_{pp} = \begin{bmatrix} \kappa_{11} & \kappa_{12} \\ \kappa_{12} & \kappa_{22} \end{bmatrix}^k, \quad \boldsymbol{\kappa}^k_{pn} = \begin{bmatrix} 0 \\ 0 \end{bmatrix}^k, \quad \boldsymbol{\kappa}^k_{np} = [\,0 \quad 0\,]^k, \quad \boldsymbol{\kappa}^k_{nn} = [\,\kappa_{33}\,]^k. \tag{46}$$

5. Principle of virtual displacements, PVD

In this section two different extensions of the Principle of Virtual Displacements (PVD) are given: the first is for the partially coupled thermo-mechanical analysis, the second one is for the fully coupled thermo-mechanical problem. In the case of a partially coupled analysis the PVD is the same of the mechanical case, but the stresses are considered as an algebraic addition of the pure mechanical and pure thermal parts [6,14]. For the fully coupled

analysis, the virtual internal thermal work is added to the virtual internal mechanical one [26,49].

5.1. PVD for the partially coupled thermo-mechanical case

In the case of the thermal stress analysis of plates, a possible extension of the PVD considers the temperature as an external load without any coupling between the mechanical and thermal fields [12]. In the variational statement obtained in Eq. (49) the stresses are seen as an algebraic addition of mechanical (d) and thermal (t) contributions:

$$\boldsymbol{\sigma}^k_{pC} = \boldsymbol{\sigma}^k_{pd} - \boldsymbol{\sigma}^k_{pt} = \mathbf{Q}^k_{pp}\boldsymbol{\epsilon}^k_{pG} + \mathbf{Q}^k_{pn}\boldsymbol{\epsilon}^k_{nG} - \boldsymbol{\lambda}^k_p\theta^k, \tag{47}$$

$$\boldsymbol{\sigma}^k_{nC} = \boldsymbol{\sigma}^k_{nd} - \boldsymbol{\sigma}^k_{nt} = \mathbf{Q}^k_{np}\boldsymbol{\epsilon}^k_{pG} + \mathbf{Q}^k_{nn}\boldsymbol{\epsilon}^k_{nG} - \boldsymbol{\lambda}^k_n\theta^k, \tag{48}$$

where the arrays $\boldsymbol{\lambda}_p$ and $\boldsymbol{\lambda}_n$ permit the partial coupling between the mechanical field and the temperature.

By considering a laminate of N_l layers, and the integral on the volume V_k of each layer k as an integral on the in-plane domain Ω_k plus the integral in the thickness direction domain A_k, it is possible to write:

$$\sum_{k=1}^{N_l}\int_{\Omega_k}\int_{A_k}\left\{\delta\boldsymbol{\epsilon}^{k\,T}_{pG}\left(\boldsymbol{\sigma}^k_{pd} - \boldsymbol{\sigma}^k_{pt}\right) + \delta\boldsymbol{\epsilon}^{k\,T}_{nG}\left(\boldsymbol{\sigma}^k_{nd} - \boldsymbol{\sigma}^k_{nt}\right)\right\}d\Omega_k\,dz = \sum_{k=1}^{N_l}\delta L^k_e - \sum_{k=1}^{N_l}\delta L^k_{in}, \tag{49}$$

where δL^k_e and δL^k_{in} are the external and inertial virtual works at the k-layer level, respectively. By substituting the Eqs. (47) and (48) in the variational statement of Eq. (49), and considering the geometrical relations for plates of Section 3, and the CUF of Section 2, for a generic layer k it is possible to write:

$$\int_{\Omega_k}\int_{A_k}\Big[\left(\mathbf{D}_p F_s\delta\mathbf{u}^k_s\right)^T\left(\mathbf{Q}^k_{pp}\mathbf{D}_p F_\tau\mathbf{u}^k_\tau + \mathbf{Q}^k_{pn}(\mathbf{D}_{np}+\mathbf{D}_{nz})F_\tau\mathbf{u}^k_\tau - \boldsymbol{\lambda}^k_p F_\tau\theta^k_\tau\right) + \left((\mathbf{D}_{np}+\mathbf{D}_{nz})F_s\delta\mathbf{u}^k_s\right)^T\left(\mathbf{Q}^k_{np}\mathbf{D}_p F_\tau\mathbf{u}^k_\tau + \mathbf{Q}^k_{nn}(\mathbf{D}_{np}+\mathbf{D}_{nz})F_\tau\mathbf{u}^k_\tau - \boldsymbol{\lambda}^k_n F_\tau\theta^k_\tau\right)\Big]d\Omega_k\,dz = \delta L^k_e - \delta L^k_{in}. \tag{50}$$

By using the integration by parts, as given in [14], the governing equations are:

$$\delta\mathbf{u}^k_s: \quad \mathbf{K}^{k\tau s}_{uu}\mathbf{u}^k_\tau = -\mathbf{M}^{k\tau s}_{uu}\ddot{\mathbf{u}}^k_\tau - \mathbf{K}^{k\tau s}_{u\theta}\theta^k_\tau + \mathbf{p}^k_{us}, \tag{51}$$

with related boundary conditions on edge Γ_k:

$$\boldsymbol{\Pi}^{k\tau s}_{uu}\mathbf{u}^k_\tau - \boldsymbol{\Pi}^{k\tau s}_{\theta\theta}\theta^k_\tau = \boldsymbol{\Pi}^{k\tau s}_{uu}\bar{\mathbf{u}}^k_\tau - \boldsymbol{\Pi}^{k\tau s}_{\theta\theta}\bar{\theta}^k_\tau, \tag{52}$$

where $\left(-\mathbf{K}^{k\tau s}_{u\theta}\theta^k_\tau\right)$ is the thermal load $\mathbf{p}^k_{\theta s}$, $\left(-\mathbf{M}^{k\tau s}_{uu}\ddot{\mathbf{u}}^k_\tau\right)$ is the inertial load and $\mathbf{p}^k_{us}$ is the external mechanical one. From Eqs. (51) and (52), simply discarding the thermal contribution, it is possible to obtain the governing equations and the boundary conditions for the pure mechanical case: the variational statement for this case is obtained from Eq. (49) simply discarding the thermal contribution for the stresses. $\mathbf{M}^{k\tau s}_{uu}$ is the inertial contribution in term of fundamental nucleus, $\mathbf{u}^k_\tau$ is the vector of the degrees of freedom for the displacements, θ^k_τ is the vector of the degrees of freedom for the temperature, $\ddot{\mathbf{u}}^k_\tau$ is the second temporal derivative of $\mathbf{u}^k_\tau$, $\mathbf{K}^{k\tau s}_{uu}$ is the fundamental nucleus for the stiffness matrix, $\mathbf{K}^{k\tau s}_{u\theta}$ is the fundamental nucleus for the thermal load. $\boldsymbol{\Pi}^{k\tau s}_{uu}$ and $\boldsymbol{\Pi}^{k\tau s}_{\theta\theta}$ are the fundamental nuclei for the boundary conditions:

$$\mathbf{K}^{k\tau s}_{uu} = \int_{A_k}\Big[(-\mathbf{D}_p)^T\left(\mathbf{Q}^k_{pp}\mathbf{D}_p + \mathbf{Q}^k_{pn}(\mathbf{D}_{np}+\mathbf{D}_{nz})\right) + (-\mathbf{D}_{np}+\mathbf{D}_{nz})^T\left(\mathbf{Q}^k_{np}\mathbf{D}_p + \mathbf{Q}^k_{nn}(\mathbf{D}_{np}+\mathbf{D}_{nz})\right)\Big]F_sF_\tau\,dz, \tag{53}$$

$$\mathbf{K}^{k\tau s}_{u\theta} = \int_{A_k}\left[(-\mathbf{D}_p)^T\left(-\boldsymbol{\lambda}^k_p\right) + (-\mathbf{D}_{np}+\mathbf{D}_{nz})^T\left(-\boldsymbol{\lambda}^k_n\right)\right]F_sF_\tau\,dz, \tag{54}$$

$$\mathbf{M}^{k\tau s}_{uu} = \int_{A_k}(\rho^k\mathbf{I})F_sF_\tau\,dz, \tag{55}$$

$$\boldsymbol{\Pi}^{k\tau s}_{uu} = \int_{A_k}\Big[\mathbf{I}^T_p\left(\mathbf{Q}^k_{pp}\mathbf{D}_p + \mathbf{Q}^k_{pn}(\mathbf{D}_{np}+\mathbf{D}_{nz})\right) + \mathbf{I}^T_{np}\left(\mathbf{Q}^k_{np}\mathbf{D}_p + \mathbf{Q}^k_{nn}(\mathbf{D}_{np}+\mathbf{D}_{nz})\right)\Big]F_sF_\tau\,dz, \tag{56}$$

$$\boldsymbol{\Pi}^{k\tau s}_{\theta\theta} = \int_{A_k}\left[\mathbf{I}^T_p\left(-\boldsymbol{\lambda}^k_p\right) + \mathbf{I}^T_{np}\left(-\boldsymbol{\lambda}^k_n\right)\right]F_sF_\tau\,dz. \tag{57}$$

ρ^k is the mass density of the kth layer and $\mathbf{I}$ is the (3×3) identity matrix. $\mathbf{I}_p$ and $\mathbf{I}_{np}$ are (3×3) matrices, to perform the integration by parts, obtained from matrices $\mathbf{D}_p$ and $\mathbf{D}_{np}$ simply replacing the differential operators with 1.

In order to define the thermal load, the temperature profile must be a priori given: by linearly assuming it in the thickness direction (θ_a) or by calculating it with solving the Fourier heat conduction equation (θ_c).

5.1.1. Assumed temperature profile, θ_a

If the values of the temperature are known at the top and bottom surface of the plate, an assumed profile $\theta(z)$, which varies linearly from the top to the bottom, is given. The temperature is assumed bi-sinusoidal in the plane (x,y) at the top and bottom plate surfaces, see Fig. 2:

$$\theta(x,y,z) = \hat{\theta}(z)\sin\left(\frac{m\pi}{a}x\right)\sin\left(\frac{n\pi}{b}y\right), \tag{58}$$

with values $\hat{\theta}(+h/2) = \theta_t$ and $\hat{\theta}(-h/2) = \theta_b$. a and b are the plate dimensions. m and n are the waves number. In the case of assumed temperature profile (θ_a) a linear through the thickness distribution is considered from θ_t to θ_b. Independently by the number of considered layers, the linear profile is always the same as indicated in Fig. 3: here examples of one-layered and two-layered plates are given for a temperature profile, in a given point in the plane, which goes from +1.0 at the top to 0.0 at the bottom. The temperature profile is approximated as displacements in case of the LW approach:

$$\theta^k(z) = F_\tau\theta^k_\tau \qquad \text{with} \qquad \tau = t,b,r \quad \text{and} \quad r = 2,\ldots,4, \tag{59}$$

t and b indicate the top and bottom of the considered kth layer. The thickness functions F_τ are a combination of Legendre polynomials (see Section 2.2).

If the temperature is assumed linear through the thickness, the values at the top and bottom surfaces, and therefore F_t and F_b, would be sufficient to describe the assumed profile via CUF (see Fig. 3) [6].

5.1.2. Calculated temperature profile, θ_c

The calculation procedure for the actual temperature profile in case of one or more layers is given in [12,14,15], in order to obtain the values of θ^k_τ for the Eq. (59). The Fourier heat conduction equation is:

$$\kappa^k_{11}\frac{\partial^2\theta}{\partial x^2} + \kappa^k_{22}\frac{\partial^2\theta}{\partial y^2} + \kappa^k_{33}\frac{\partial^2\theta}{\partial z^2} = 0, \tag{60}$$

it is solved in the case of plate subjected to a bi-sinusoidal temperature at the top and at the bottom. The thermal boundary conditions are:

$$\begin{aligned}
&\theta = 0 \qquad \text{at} \qquad x = 0,a \quad \text{and} \quad y = 0,b,\\
&\theta = \theta_b\sin\left(\frac{m\pi x}{a}\right)\sin\left(\frac{n\pi y}{b}\right) \qquad \text{at} \qquad z = -\frac{h}{2} \quad \text{with} \quad b: \text{bottom},\\
&\theta = \theta_t\sin\left(\frac{m\pi x}{a}\right)\sin\left(\frac{n\pi y}{b}\right) \qquad \text{at} \qquad z = +\frac{h}{2} \quad \text{with} \quad t: \text{top},
\end{aligned} \tag{61}$$

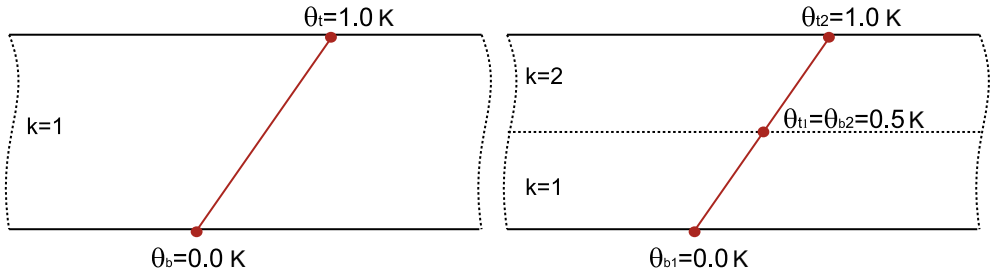

Fig. 3. Assumed linear sovra-temperature profile (θ_a) through the thickness direction of a one-layered and a two-layered plate.

where m and n are the waves number along the two in-plane plate directions (x,y). a and b are the plate dimensions, h is the plate thickness, and θ_b and θ_t are the amplitudes of the temperature at the bottom and top of each layer, respectively.

We compute the temperature θ_c at different values z_N in the thickness of the multilayered plate by solving the Eq. (60) with the boundary conditions in Eq. (61). By solving the system in Eq. (62), we obtain the N values of θ_τ^k for the CUF:

$$\begin{bmatrix} \theta_c(z_1) \\ \theta_c(z_2) \\ \vdots \\ \theta_c(z_N) \end{bmatrix} = \begin{bmatrix} F_0(z_1) & F_1(z_1) & \cdots & F_N(z_1) \\ F_0(z_2) & F_1(z_2) & \cdots & F_N(z_2) \\ \vdots & \vdots & \vdots & \vdots \\ F_0(z_N) & F_1(z_N) & \cdots & F_N(z_N) \end{bmatrix} \begin{bmatrix} \theta_0^k \\ \theta_1^k \\ \vdots \\ \theta_N^k \end{bmatrix}. \tag{62}$$

Therefore, if we consider a generic multilayered plate, the temperature profile is approximated by Eq. (59) and the N values of θ_τ^k are given by Eq. (62). The details, here omitted for sake of brevity, can be found in [12,14,15].

5.2. PVD for the fully coupled thermo-mechanical case

In case of fully coupling between the thermal and mechanical fields, the variational statement is the PVD with the introduction of the virtual internal thermal work. This variational statement is:

$$\int_V \left(\delta\boldsymbol{\epsilon}_{pG}^T \boldsymbol{\sigma}_{pC} + \delta\boldsymbol{\epsilon}_{nG}^T \boldsymbol{\sigma}_{nC} - \delta\theta\eta_C - \delta\boldsymbol{\vartheta}_{pG}^T \boldsymbol{h}_{pC} - \delta\boldsymbol{\vartheta}_{nG}^T \boldsymbol{h}_{nC} \right) dV = \delta L_e - \delta L_{in}. \tag{63}$$

By considering a laminate of N_l layers and the volume V_k for each layer k as an integral on the in-plane surface Ω_k and an integral in the thickness direction domain A_k, the Eq. (63) can be rewritten as:

$$\sum_{k=1}^{N_l} \int_{\Omega_k} \int_{A_k} \left\{ \delta\boldsymbol{\epsilon}_{pG}^{k\,T} \boldsymbol{\sigma}_{pC}^k + \delta\boldsymbol{\epsilon}_{nG}^{k\,T} \boldsymbol{\sigma}_{nC}^k - \delta\theta^k \eta_C^k - \delta\boldsymbol{\vartheta}_{pG}^{k\,T} \boldsymbol{h}_{pC}^k - \delta\boldsymbol{\vartheta}_{nG}^{k\,T} \boldsymbol{h}_{nC}^k \right\} d\Omega_k\, dz = \sum_{k=1}^{N_l} \delta L_e^k - \sum_{k=1}^{N_l} \delta L_{in}^k, \tag{64}$$

where δL_e^k and δL_{in}^k are the external and inertial virtual work at the k-layer level, respectively.

The governing equations have the following form:

$$\begin{aligned} \delta\boldsymbol{u}_s^k: &\quad \boldsymbol{K}_{uu}^{k\tau s}\boldsymbol{u}_\tau^k + \boldsymbol{K}_{u\theta}^{k\tau s}\theta_\tau^k = \boldsymbol{p}_{us}^k - \boldsymbol{M}_{uu}^{k\tau s}\ddot{\boldsymbol{u}}_\tau^k, \\ \delta\theta_s^k: &\quad \boldsymbol{K}_{\theta u}^{k\tau s}\boldsymbol{u}_\tau^k + \boldsymbol{K}_{\theta\theta}^{k\tau s}\theta_\tau^k = \boldsymbol{p}_{\theta s}^k. \end{aligned} \tag{65}$$

The arrays $\boldsymbol{p}_{us}^k$ and $\boldsymbol{p}_{\theta s}^k$ indicate the variationally consistent mechanical and thermal loadings, respectively. Along with these governing equations the following boundary conditions on the edge Γ_k of the in-plane integration domain Ω_k hold:

$$\begin{aligned} \boldsymbol{\Pi}_{uu}^{k\tau s}\boldsymbol{u}_\tau^k + \boldsymbol{\Pi}_{u\theta}^{k\tau s}\theta_\tau^k &= \boldsymbol{\Pi}_{uu}^{k\tau s}\bar{\boldsymbol{u}}_\tau^k + \boldsymbol{\Pi}_{u\theta}^{k\tau s}\bar{\theta}_\tau^k, \\ \boldsymbol{\Pi}_{\theta u}^{k\tau s}\boldsymbol{u}_\tau^k + \boldsymbol{\Pi}_{\theta\theta}^{k\tau s}\theta_\tau^k &= \boldsymbol{\Pi}_{\theta u}^{k\tau s}\bar{\boldsymbol{u}}_\tau^k + \boldsymbol{\Pi}_{\theta\theta}^{k\tau s}\bar{\theta}_\tau^k. \end{aligned} \tag{66}$$

As indicated in [26], the sovra-temperature θ^k is a variable of the problem. The displacements $\boldsymbol{u}^k$ can be seen in ESL or LW form. Independently by the choice made for the displacements, the sovra-temperature is always seen in LW form.

As discussed in [17,19], the variational statement includes only the internal thermal work made by the gradient of temperature in the case of temperature applied at the top and bottom of the structure; it includes only the internal thermal work made by the temperature in the case of mechanical load applied on the structure or free vibration problem.

5.2.1. Imposed temperature on the surfaces

In case of temperature imposed at the top and bottom of the structure, in the Eq. (64) the term $\delta\theta^k\eta_C^k$ is not considered because it does not exist a virtual variation of temperature. Therefore, the variational statement is:

$$\sum_{k=1}^{N_l} \int_{\Omega_k} \int_{A_k} \left\{ \delta\boldsymbol{\epsilon}_{pG}^{k\,T} \boldsymbol{\sigma}_{pC}^k + \delta\boldsymbol{\epsilon}_{nG}^{k\,T} \boldsymbol{\sigma}_{nC}^k - \delta\boldsymbol{\vartheta}_{pG}^{k\,T} \boldsymbol{h}_{pC}^k - \delta\boldsymbol{\vartheta}_{nG}^{k\,T} \boldsymbol{h}_{nC}^k \right\} d\Omega_k\, dz = \sum_{k=1}^{N_l} \delta L_e^k - \sum_{k=1}^{N_l} \delta L_{in}^k. \tag{67}$$

From the constitutive equations, as obtained in Eqs. (39)–(43), simply discarding the entropy η_c^k:

$$\boldsymbol{\sigma}_{pC}^k = \boldsymbol{Q}_{pp}^k \boldsymbol{\epsilon}_{pG}^k + \boldsymbol{Q}_{pn}^k \boldsymbol{\epsilon}_{nG}^k - \boldsymbol{\lambda}_p^k \theta^k, \tag{68}$$

$$\boldsymbol{\sigma}_{nC}^k = \boldsymbol{Q}_{np}^k \boldsymbol{\epsilon}_{pG}^k + \boldsymbol{Q}_{nn}^k \boldsymbol{\epsilon}_{nG}^k - \boldsymbol{\lambda}_n^k \theta^k, \tag{69}$$

$$\boldsymbol{h}_{pC}^k = \boldsymbol{\kappa}_{pp}^k \boldsymbol{\vartheta}_{pG}^k + \boldsymbol{\kappa}_{pn}^k \boldsymbol{\vartheta}_{nG}^k, \tag{70}$$

$$\boldsymbol{h}_{nC}^k = \boldsymbol{\kappa}_{np}^k \boldsymbol{\vartheta}_{pG}^k + \boldsymbol{\kappa}_{nn}^k \boldsymbol{\vartheta}_{nG}^k. \tag{71}$$

The geometrical relations for plates have been obtained in Section 3, and Carrera's Unified Formulation is described in Section 2. The Eq. (67) is rewritten in the following form in the case of a generic layer k:

$$\begin{aligned} \int_{\Omega_k} \int_{A_k} \Big[& \left(\boldsymbol{D}_p F_s \delta\boldsymbol{u}_s^k\right)^T \left(\left(\boldsymbol{Q}_{pp}^k \boldsymbol{D}_p + \boldsymbol{Q}_{pn}^k (\boldsymbol{D}_{np} + \boldsymbol{D}_{nz}) \right) F_\tau \boldsymbol{u}_\tau^k - \boldsymbol{\lambda}_p^k F_\tau \theta_\tau^k \right) \\ & + \left((\boldsymbol{D}_{np} + \boldsymbol{D}_{nz}) F_s \delta\boldsymbol{u}_s^k \right)^T \left(\left(\boldsymbol{Q}_{np}^k \boldsymbol{D}_p + \boldsymbol{Q}_{nn}^k (\boldsymbol{D}_{np} + \boldsymbol{D}_{nz}) \right) F_\tau \boldsymbol{u}_\tau^k - \boldsymbol{\lambda}_n^k F_\tau \theta_\tau^k \right) \\ & + \left(\boldsymbol{D}_{tp} F_s \delta\theta_s^k \right)^T \left(\left(\boldsymbol{\kappa}_{pp}^k (-\boldsymbol{D}_{tp}) + \boldsymbol{\kappa}_{pn}^k (-\boldsymbol{D}_{tn}) \right) F_\tau \theta_\tau^k \right) + \left(\boldsymbol{D}_{tn} F_s \delta\theta_s^k \right)^T \\ & \times \left(\left(\boldsymbol{\kappa}_{np}^k (-\boldsymbol{D}_{tp}) + \boldsymbol{\kappa}_{nn}^k (-\boldsymbol{D}_{tn}) \right) F_\tau \theta_\tau^k \right) \Big] d\Omega_k\, dz = \delta L_e^k - \delta L_{in}^k. \end{aligned} \tag{72}$$

Integrating by parts the Eq. (72), as suggested in [12,14], the fundamental nuclei are:

$$\begin{aligned} \boldsymbol{K}_{uu}^{k\tau s} = \int_{A_k} \Big[& (-\boldsymbol{D}_p)^T \left(\boldsymbol{Q}_{pp}^k \boldsymbol{D}_p + \boldsymbol{Q}_{pn}^k (\boldsymbol{D}_{np} + \boldsymbol{D}_{nz}) \right) \\ & + (-\boldsymbol{D}_{np} + \boldsymbol{D}_{nz})^T \left(\boldsymbol{Q}_{np}^k \boldsymbol{D}_p + \boldsymbol{Q}_{nn}^k (\boldsymbol{D}_{np} + \boldsymbol{D}_{nz}) \right) \Big] F_s F_\tau\, dz, \end{aligned} \tag{73}$$

$$\boldsymbol{K}_{u\theta}^{k\tau s} = \int_{A_k} \left[(-\boldsymbol{D}_p)^T \left(-\boldsymbol{\lambda}_p^k \right) + (-\boldsymbol{D}_{np} + \boldsymbol{D}_{nz})^T \left(-\boldsymbol{\lambda}_n^k \right) \right] F_s F_\tau\, dz, \tag{74}$$

$$\boldsymbol{K}_{\theta u}^{k\tau s} = 0 \tag{75}$$

$$\boldsymbol{K}_{\theta\theta}^{k\tau s} = \int_{A_k} \left[\boldsymbol{D}_{tp}^T \boldsymbol{\kappa}_{pp}^k \boldsymbol{D}_{tp} + \boldsymbol{D}_{tp}^T \boldsymbol{\kappa}_{pn}^k \boldsymbol{D}_{tn} - \boldsymbol{D}_{tn}^T \boldsymbol{\kappa}_{np}^k \boldsymbol{D}_{tp} - \boldsymbol{D}_{tn}^T \boldsymbol{\kappa}_{nn}^k \boldsymbol{D}_{tn} \right] F_s F_\tau \, dz. \tag{76}$$

The fundamental nuclei $\boldsymbol{K}_{uu}^{k\tau s}$ and $\boldsymbol{K}_{u\theta}^{k\tau s}$ are the same obtained in Section 5.1 for the partially coupled problem. The nuclei for boundary conditions on the edge Γ_k are:

$$\boldsymbol{\Pi}_{uu}^{k\tau s} = \int_{A_k} \left[\boldsymbol{I}_p^T \left(\boldsymbol{Q}_{pp}^k \boldsymbol{D}_p + \boldsymbol{Q}_{pn}^k (\boldsymbol{D}_{np} + \boldsymbol{D}_{nz}) \right) + \boldsymbol{I}_{np}^T \left(\boldsymbol{Q}_{np}^k \boldsymbol{D}_p + \boldsymbol{Q}_{nn}^k (\boldsymbol{D}_{np} + \boldsymbol{D}_{nz}) \right) \right] F_s F_\tau \, dz, \tag{77}$$

$$\boldsymbol{\Pi}_{u\theta}^{k\tau s} = \int_{A_k} \left[\boldsymbol{I}_p^T \left(-\boldsymbol{\lambda}_p^k \right) + \boldsymbol{I}_{np}^T \left(-\boldsymbol{\lambda}_n^k \right) \right] F_s F_\tau \, dz, \tag{78}$$

$$\boldsymbol{\Pi}_{\theta u}^{k\tau s} = 0 \tag{79}$$

$$\boldsymbol{\Pi}_{\theta\theta}^{k\tau s} = \int_{A_k} \left[\boldsymbol{I}_{tp}^T \boldsymbol{\kappa}_{pp}^k (-\boldsymbol{D}_{tp}) + \boldsymbol{I}_{tp}^T \boldsymbol{\kappa}_{pn}^k (-\boldsymbol{D}_{tn}) \right] F_s F_\tau \, dz. \tag{80}$$

The fundamental nuclei $\boldsymbol{\Pi}_{uu}^{k\tau s}$ and $\boldsymbol{\Pi}_{u\theta}^{k\tau s}$ are the same obtained in Section 5.1 for the partially coupled problem. $\boldsymbol{I}_{np}$ (2×1) and $\boldsymbol{I}_{tp}$ (1×1) are matrices, to perform the integration by parts, obtained from $\boldsymbol{D}_{np}$ and $\boldsymbol{D}_{tp}$ simply replacing the differential operator with 1. Nuclei, given in Eqs. (73)–(76) are introduced in the governing Eq. (65) in the case of temperature applied on the plate surfaces. In this case, in Eq. (65) the inertial contribute and the mechanical load are discarded. The sovra-temperature is directly imposed in the vector θ_τ^k; therefore, the thermal load $\boldsymbol{p}_{\theta s}^k$ is not considered.

5.2.2. Mechanical load and free vibration analysis

In case of mechanical load applied on the structure or free vibration analysis, in the Eq. (64) the terms $\delta \vartheta_{pG}^{k\,T} \boldsymbol{h}_{pC}^k$ and $\delta \vartheta_{nG}^{k\,T} \boldsymbol{h}_{nC}^k$ are not considered because it does not exist a gradient of temperature variation. Therefore, the variational statement is:

$$\sum_{k=1}^{N_l} \int_{\Omega_k} \int_{A_k} \left\{ \delta \boldsymbol{\epsilon}_{pG}^{k\,T} \boldsymbol{\sigma}_{pC}^k + \delta \boldsymbol{\epsilon}_{nG}^{k\,T} \boldsymbol{\sigma}_{nC}^k - \delta\theta^k \eta_C^k \right\} d\Omega_k \, dz = \sum_{k=1}^{N_l} \delta L_e^k - \sum_{k=1}^{N_l} \delta L_{in}^k. \tag{81}$$

By considering the constitutive equations as obtained in Eqs. (39)–(43), simply discarding the heat fluxes $\boldsymbol{h}_{pC}^k$ and $\boldsymbol{h}_{nC}^k$:

$$\boldsymbol{\sigma}_{pC}^k = \boldsymbol{Q}_{pp}^k \boldsymbol{\epsilon}_{pG}^k + \boldsymbol{Q}_{pn}^k \boldsymbol{\epsilon}_{nG}^k - \boldsymbol{\lambda}_p^k \theta^k, \tag{82}$$

$$\boldsymbol{\sigma}_{nC}^k = \boldsymbol{Q}_{np}^k \boldsymbol{\epsilon}_{pG}^k + \boldsymbol{Q}_{nn}^k \boldsymbol{\epsilon}_{nG}^k - \boldsymbol{\lambda}_n^k \theta^k, \tag{83}$$

$$\eta_C^k = \boldsymbol{\lambda}_p^{kT} \boldsymbol{\epsilon}_{pG}^k + \boldsymbol{\lambda}_n^{kT} \boldsymbol{\epsilon}_{nG}^k + \chi^k \theta^k. \tag{84}$$

The geometrical relations for plates have been obtained in Section 3, Carrera's Unified Formulation is described in Section 2. The Eq. (81) is rewritten in the following form for a generic layer k:

$$\int_{\Omega_k} \int_{A_k} \left[\left(\boldsymbol{D}_p F_s \delta \boldsymbol{u}_s^k \right)^T \left(\left(\boldsymbol{Q}_{pp}^k \boldsymbol{D}_p + \boldsymbol{Q}_{pn}^k (\boldsymbol{D}_{np} + \boldsymbol{D}_{nz}) \right) F_\tau \boldsymbol{u}_\tau^k - \boldsymbol{\lambda}_p^k F_\tau \theta_\tau^k \right) + \left((\boldsymbol{D}_{np} + \boldsymbol{D}_{nz}) F_s \delta \boldsymbol{u}_s^k \right)^T \left(\left(\boldsymbol{Q}_{np}^k \boldsymbol{D}_p + \boldsymbol{Q}_{nn}^k (\boldsymbol{D}_{np} + \boldsymbol{D}_{nz}) \right) F_\tau \boldsymbol{u}_\tau^k - \boldsymbol{\lambda}_n^k F_\tau \theta_\tau^k \right) - F_s \delta \theta_s^{kT} \left(\left(\boldsymbol{\lambda}_p^{kT} \boldsymbol{D}_p + \boldsymbol{\lambda}_n^{kT} (\boldsymbol{D}_{np} + \boldsymbol{D}_{nz}) \right) F_\tau \boldsymbol{u}_\tau^k + \chi^k F_\tau \theta_\tau^k \right) \right] d\Omega_k \, dz = \delta L_e^k - \delta L_{in}^k. \tag{85}$$

Integrating by parts the Eq. (85), as suggested in [12,14], the fundamental nuclei $\boldsymbol{K}_{uu}^{k\tau s}$ and $\boldsymbol{K}_{u\theta}^{k\tau s}$ are the same of PVD in Sections 5.1 and 5.2.1, while nuclei $\boldsymbol{K}_{\theta u}^{k\tau s}$ and $\boldsymbol{K}_{\theta\theta}^{k\tau s}$ are:

$$\boldsymbol{K}_{\theta u}^{k\tau s} = \int_{A_k} \left[-\boldsymbol{\lambda}_p^{kT} \boldsymbol{D}_p - \boldsymbol{\lambda}_n^{kT} (\boldsymbol{D}_{np} + \boldsymbol{D}_{nz}) \right] F_s F_\tau \, dz, \tag{86}$$

$$\boldsymbol{K}_{\theta\theta}^{k\tau s} = \int_{A_k} [-\chi^k] F_s F_\tau \, dz. \tag{87}$$

Nuclei for boundary conditions on the edge Γ_k, $\boldsymbol{\Pi}_{uu}^{k\tau s}$ and $\boldsymbol{\Pi}_{u\theta}^{k\tau s}$, are the same of PVD in Sections 5.1 and 5.2.1, while the other two state:

$$\boldsymbol{\Pi}_{\theta u}^{k\tau s} = \boldsymbol{\Pi}_{\theta\theta}^{k\tau s} = 0. \tag{88}$$

Nuclei, here obtained, are introduced in the governing Eq. (65) in the case of mechanical load applied on the plate surfaces or free vibration analysis. In this case, in Eq. (65) the thermal load is discarded. Fundamental nucleus for the inertial contribute is the same already obtained in Eq. (55) of Section 5.1.

6. Navier solution and assembling procedure

In order to write the explicit form of fundamental nuclei obtained in Sections 5.1 and 5.2, the following integrals in the z-thickness direction must be defined:

$$(J^{k\tau s}, J^{k\tau_z s}, J^{k\tau s_z}, J^{k\tau_z s_z}) = \int_{A_k} \left(F_\tau F_s, \frac{\partial F_\tau}{\partial z} F_s, F_\tau \frac{\partial F_s}{\partial z}, \frac{\partial F_\tau}{\partial z} \frac{\partial F_s}{\partial z} \right) dz. \tag{89}$$

By using the Eq. (89) and developing the matrices products, the explicit forms of fundamental nuclei are obtained.

Navier-type closed-form solution is obtained via substitution of harmonic expressions for the displacements and temperature as well as considering the following material coefficients equal zero: $Q_{16} = Q_{26} = Q_{36} = Q_{45} = 0$ and $\lambda_6 = \kappa_{12} = 0$. The following harmonic assumptions can be made for the variables, which correspond to simply supported boundary conditions:

$$\begin{aligned} u_\tau^k &= \sum_{m,n} \left(\widehat{U}_\tau^k \right) \cos\left(\frac{m\pi x}{a} \right) \sin\left(\frac{n\pi y}{b} \right), \quad k = 1, N_l, \\ v_\tau^k &= \sum_{m,n} \left(\widehat{V}_\tau^k \right) \sin\left(\frac{m\pi x}{a} \right) \cos\left(\frac{n\pi y}{b} \right), \quad \tau = t, b, r, \\ \left(w_\tau^k, \theta_\tau^k \right) &= \sum_{m,n} \left(\widehat{W}_\tau^k, \hat{\theta}_\tau^k \right) \sin\left(\frac{m\pi x}{a} \right) \sin\left(\frac{n\pi y}{b} \right), \quad r = 2, N, \end{aligned} \tag{90}$$

where $\widehat{U}_\tau^k$, $\widehat{V}_\tau^k$, $\widehat{W}_\tau^k$, $\hat{\theta}_\tau^k$ are the amplitudes.

Fundamental nucleus $\boldsymbol{K}_{uu}^{k\tau s}$, of dimension (3×3), is in common for each considered case:

$$\begin{aligned} K_{uu_{11}} &= Q_{55}^k J^{k\tau_z s_z} + Q_{11}^k J^{k\tau s} \bar{\alpha}^2 + Q_{66}^k J^{k\tau s} \bar{\beta}^2, \\ K_{uu_{12}} &= J^{k\tau s} \bar{\alpha} \bar{\beta} \left(Q_{12}^k + Q_{66}^k \right) = K_{uu_{21}}, \\ K_{uu_{13}} &= Q_{55}^k J^{k\tau_z s} \bar{\alpha} - Q_{13}^k J^{k\tau s_z} \bar{\alpha}, \quad K_{uu_{22}} = Q_{44}^k J^{k\tau_z s_z} + Q_{22}^k J^{k\tau s} \bar{\beta}^2 + Q_{66}^k J^{k\tau s} \bar{\alpha}^2, \\ K_{uu_{23}} &= Q_{44}^k J^{k\tau_z s} \bar{\beta} - Q_{23}^k J^{k\tau s_z} \bar{\beta}, \quad K_{uu_{31}} = Q_{55}^k J^{k\tau s_z} \bar{\alpha} - Q_{13}^k J_\beta^{k\tau_z s} \bar{\alpha}, \\ K_{uu_{32}} &= Q_{44}^k J_\alpha^{k\tau s_z} \bar{\beta} - Q_{23}^k J^{k\tau_z s} \bar{\beta}, \quad K_{uu_{33}} = Q_{55}^k J^{k\tau s} \bar{\alpha}^2 + Q_{44}^k J^{k\tau s} \bar{\beta}^2 + Q_{33}^k J^{k\tau_z s_z}. \end{aligned} \tag{91}$$

Fundamental nucleus $\boldsymbol{K}_{u\theta}^{k\tau s}$, of dimension (3×1), is in common for the partially coupled case and for each extension of the fully coupled case:

$$K_{u\theta_{11}} = \bar{\alpha} J^{k\tau s} \lambda_1^k, \quad K_{u\theta_{21}} = \bar{\beta} J^{k\tau s} \lambda_2^k, \quad K_{u\theta_{31}} = -J^{k\tau_z s} \lambda_3^k. \tag{92}$$

Fundamental nuclei $\boldsymbol{K}_{\theta u}^{k\tau s}$, of dimension (1×3), and $\boldsymbol{K}_{\theta\theta}^{k\tau s}$, of dimension (1×1), for the fully coupled thermo-mechanical analysis, in the case of applied temperature on the surfaces, are:

$$K_{\theta u_{11}} = K_{\theta u_{12}} = K_{\theta u_{13}} = 0, \tag{93}$$

$$K_{\theta\theta_{11}} = -J^{k\tau s} \bar{\alpha}^2 \kappa_{11} - J^{k\tau s} \bar{\beta}^2 \kappa_{22} - J^{k\tau_z s_z} \kappa_{33}. \tag{94}$$

Fundamental nuclei $\boldsymbol{K}_{\theta u}^{k\tau s}$, of dimension (1×3), and $\boldsymbol{K}_{\theta\theta}^{k\tau s}$, of dimension (1×1), for the fully coupled thermo-mechanical analysis, in the case of applied mechanical load and free vibration problem, are:

$$K_{\theta u_{11}} = \bar{\alpha} J^{k\tau s} \lambda_1^k, \quad K_{\theta u_{12}} = \bar{\beta} J^{k\tau s} \lambda_2^k, \quad K_{\theta u_{13}} = -J^{k\tau_z s} \lambda_3^k, \tag{95}$$

$$K_{\theta\theta_{11}} = -J^{k\tau s} \chi. \tag{96}$$

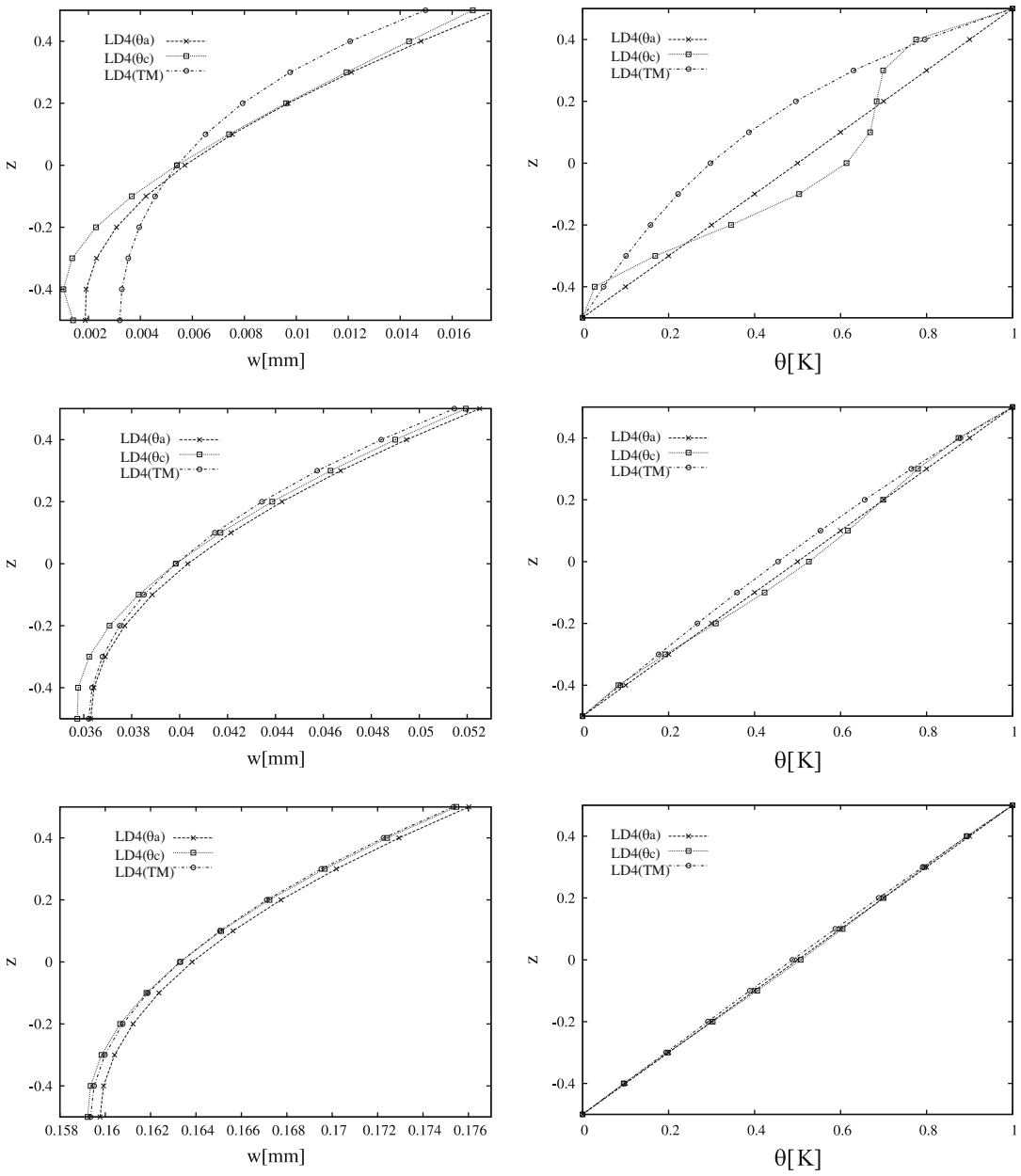

Fig. 4. One-layered isotropic plate with sovra-temperature applied on its top and bottom surfaces. Displacement w and sovra-temperature θ vs. z for $a/h = 2, 5, 10$ (top, middle and bottom figures, respectively).

The fundamental nucleus of the inertial matrix $\boldsymbol{M}_{uu}^{k\tau s}$, of dimension (3×3), is:

$$\begin{aligned} &M_{uu_{11}} = \rho^k J^{k\tau s}, \quad M_{uu_{12}} = M_{uu_{13}} = 0, \\ &M_{uu_{21}} = 0, \quad M_{uu_{22}} = \rho^k J^{k\tau s}, \quad M_{uu_{23}} = 0, \\ &M_{uu_{31}} = M_{uu_{32}} = 0, \quad M_{uu_{33}} = \rho^k J^{k\tau s}. \end{aligned} \tag{97}$$

For each proposed fundamental nucleus, $\bar{\alpha} = m\pi/a$ and $\bar{\beta} = n\pi/b$, where m and n are the wave numbers in in-plane directions, and a and b the plate dimensions.

By starting from the fundamental nuclei described in this section, matrices can be obtained for the considered multilayered plates by simply expanding and assembling via the indexes k, τ, s. By expanding via indexes τ, s, the order of expansion N from 1 to 4 in the thickness direction is considered. The matrices are obtained for each considered layer, and the index k permits the multilayer assembling procedure, which can either be ESL or LW.

6.1. Acronyms

A system of acronyms is here given in order to define the several refined two-dimensional models developed in this work. The choice made in this paper is that displacements can be in ESL or LW form, but the temperature is always considered in LW form. Therefore, a two-dimensional model is defined as ESL or LW, depending on the choice made for the displacement. ESL models are indicated as ED1–ED4, where E means the ESL approach, D means that the Principle of Virtual Displacements or their extensions to thermo-mechanical analysis have been employed; the last digit, from 1 to 4, indicates the order of expansion in the thickness direction for both displacements and temperature. In the case of LW models, the letter E is replaced by a letter L, therefore the relative models are indicated as LD1–LD4. In the case of a thermo-mechanical analysis, additional parenthesis are introduced in the acronyms: (θ_a) is added in the case of partially coupled

thermo-mechanical analysis with a linear assumed temperature profile; (θ_c) is used to indicate the case of partially coupled thermo-mechanical analysis with a calculated temperature profile; (TM) means a fully coupled thermo(T)-mechanical(M) analysis. No parenthesis are added in the case of a pure mechanical problem.

7. Results

The results given in this section, consider three different cases: – plates with imposed temperature at the two external surfaces; – plates subjected to a mechanical load on their top surfaces; – free vibration analysis of plates. The considered square ($a = b$) plates, with total thickness $h = 1$ m, are simply supported. The investigated thickness ratios are $a/h = 2, 5, 10, 50$ and 100. Three different layered plates are investigated for each proposed problem. The first is a one-layered isotropic plate in Al2024 with Young's modulus $E = 73$ GPa, Poisson's ratio $\nu = 0.3$ and mass density $\rho = 2800$ Kg/m^3. The thermal properties are the specific heat per unit mass $C_\nu = 897$ J/Kg K, the thermal expansion coefficient $\alpha = 25 \times 10^{-6}$ 1/K and the conductivity coefficient $\kappa = 130$ W/mK. The two-layered isotropic plate has two layers of thickness $h_1 = h_2 = h/2 = 0.5$ m, the bottom layer is in Al2024 and the top layer is in Ti22. The mechanical properties of the Ti22 layer are $E = 110$ GPa, $\nu = 0.32$ and $\rho = 4420$ Kg/m^3. Its thermal properties are $C_\nu = 560$ J/Kg K, $\alpha = 8.6 \times 10^{-6}$ 1/K and $\kappa = 21.9$ W/mK. The third case is a two-layered composite (0°/90°) plate where the two layers have the same thickness $h_1 = h_2 = h/2 = 0.5$ m. The elastic properties of the embedded carbon fibre reinforced layers are Young's longitudinal modulus $E_1 = 172.72$ GPa, Young's transverse modulus $E_2 = E_3 = 6.909$ GPa, Poisson's ratio $\nu = 0.25$, shear modulus $G_{12} = G_{13} = 3.45$ GPa and $G_{23} = 1.38$ GPa, mass density $\rho = 1940$ Kg/m^3. The thermal properties are the specific heat per unit mass $C_\nu = 846$ J/Kg K, longitudinal thermal expansion coefficient $\alpha_1 = 0.57 \times 10^{-6}$ 1/K, transverse thermal expansion coefficients $\alpha_2 = \alpha_3 = 35.6 \times 10^{-6}$ 1/K, longitudinal conductivity coefficient $\kappa_{11} = 36.42$ W/mK and transverse conductivity coefficients $\kappa_{22} = \kappa_{33} = 0.96$ W/mK.

7.1. Imposed temperature on the surfaces

The considered plates have an imposed sovra-temperature at the top $\theta_t = 1.0$ K and at the bottom $\theta_b = 0.0$ K. The temperature is bi-sinusoidal in the in-plane directions with wave numbers $m = n = 1$. The partially coupled models ED1—ED4(θ_a), LD1—LD4(θ_a), FSDT—CLT(θ_a) and ED1—ED4(θ_c), LD1—LD4(θ_c), FSDT—CLT(θ_c) have been validated extensively in the authors' previous works [6,11,12,14,15]. In the partially coupled models, the temperature profile must be a priori defined: – assuming it linear through the thickness (θ_a) from $\theta_t = 1.0$ K to $\theta_b = 0.0$ K (see Fig. 3); – calculating it by solving the Fourier heat conduction equation (θ_c) where the thermal boundary conditions are $\theta_t = 1.0$ K at the top $\theta_b = 0.0$ K at the bottom. The temperature profile permits the thermal load to be obtained for Eq. (51). In the fully coupled models, the sovra-temperature is directly imposed in the vector θ_τ^k and the displacement and temperature profile are directly obtained by solving the governing Eq. (65).

A one-layered isotropic plate is investigated in Tables 1 and 2, and in Fig. 4. The plate has only one layer, therefore no differences can be observed for the ESL and LW theories with the same order of expansion N. Table 1 gives the transverse displacement w in the middle of the plate, Table 2 gives the in-plane displacement u at the top of the plate. When the plate is thick, the temperature profile is not linear, even when the plate is isotropic and one-layered, see Fig. 4. For thin plates, the temperature profile is linear in the thickness direction. For thick plates, displacements obtained with partially coupled models (θ_a) are different from those obtained with partially coupled (θ_c) or fully coupled models (TM) (an error due to the assumption of a linear temperature profile). When the plate is thin, the three models are coincident because the temperature profile is linear, as indicated in Fig. 4. Classical theories, such as CLT and FSDT, give very large errors for each proposed model (θ_a, θ_c and TM), even when the plate is thin: their degrees of freedom are not sufficient to exhaustively model the thermal part. The

Table 1
One-layered isotropic plate with sovra-temperature applied on its top and bottom surfaces. Displacement w in [mm] for several two-dimensional theories and thickness ratios.

	a/h	2	5	10	50	100
LD4(θ_a)	$w(0)$	0.0057	0.0403	0.1638	4.1154	16.464
LD4(θ_c)	$w(0)$	0.0054	0.0398	0.1633	4.1148	16.463
LD4(TM)	$w(0)$	0.0054	0.0398	0.1633	4.1148	16.463
LD2(θ_a)	$w(0)$	0.0053	0.0399	0.1634	4.1149	16.463
LD2(θ_c)	$w(0)$	0.0053	0.0399	0.1634	4.1149	16.463
LD2(TM)	$w(0)$	0.0053	0.0399	0.1634	4.1149	16.463
FSDT(θ_a)	$w(0)$	0.0092	0.0578	0.2311	5.7785	23.114
FSDT(θ_c)	$w(0)$	0.0092	0.0578	0.2311	5.7785	23.114
FSDT(TM)	$w(0)$	0.0092	0.0578	0.2311	5.7785	23.114
CLT(θ_a)	$w(0)$	0.0092	0.0578	0.2311	5.7785	23.114
CLT(θ_c)	$w(0)$	0.0092	0.0578	0.2311	5.7785	23.114
CLT(TM)	$w(0)$	0.0092	0.0578	0.2311	5.7785	23.114

Table 2
One-layered isotropic plate with sovra-temperature applied on its top and bottom surfaces. Displacement u in [mm] for several two-dimensional theories and thickness ratios.

	a/h	2	5	10	50	100
LD4(θ_a)	$u(h/2)$	−0.0125	−0.0269	−0.0522	−0.2587	−0.5173
LD4(θ_c)	$u(h/2)$	−0.0119	−0.0267	−0.0521	−0.2587	−0.5173
LD4(TM)	$u(h/2)$	−0.0103	−0.0259	−0.0517	−0.2586	−0.5172
LD2(θ_a)	$u(h/2)$	−0.0121	−0.0267	−0.0522	−0.2587	−0.5173
LD2(θ_c)	$u(h/2)$	−0.0107	−0.0259	−0.0517	−0.2586	−0.5172
LD2(TM)	$u(h/2)$	−0.0106	−0.0259	−0.0517	−0.2586	−0.5172
FSDT(θ_a)	$u(h/2)$	−0.0145	−0.0363	−0.0726	−0.3631	−0.7261
FSDT(θ_c)	$u(h/2)$	−0.0145	−0.0363	−0.0726	−0.3631	−0.7261
FSDT(TM)	$u(h/2)$	−0.0145	−0.0363	−0.0726	−0.3631	−0.7261
CLT(θ_a)	$u(h/2)$	−0.0145	−0.0363	−0.0726	−0.3631	−0.7261
CLT(θ_c)	$u(h/2)$	−0.0145	−0.0363	−0.0726	−0.3631	−0.7261
CLT(TM)	$u(h/2)$	−0.0145	−0.0363	−0.0726	−0.3631	−0.7261

Table 3
Two-layered isotropic plate with sovra-temperature applied on its top and bottom surfaces. Displacement w in [mm] for several two-dimensional theories and thickness ratios.

	a/h	2	5	10	50	100
LD4(θ_a)	$w(0)$	0.0016	0.0078	0.0294	0.7191	2.8747
LD4(θ_c)	$w(0)$	0.0021	0.0131	0.0517	1.2858	5.1425
LD4(TM)	$w(0)$	0.0020	0.0130	0.0516	1.2857	5.1424
ED4(θ_a)	$w(0)$	0.0011	0.0073	0.0289	0.7208	2.8828
ED4(θ_c)	$w(0)$	0.0019	0.0129	0.0516	1.2870	5.1477
ED4(TM)	$w(0)$	0.0019	0.0128	0.0514	1.2869	5.1475
LD2(θ_a)	$w(0)$	0.0016	0.0078	0.0294	0.7192	2.8747
LD2(θ_c)	$w(0)$	0.0020	0.0130	0.0516	1.2857	5.1424
LD2(TM)	$w(0)$	0.0020	0.0130	0.0516	1.2857	5.1424
FSDT(θ_a)	$w(0)$	0.0018	0.0111	0.0443	1.1073	4.4292
FSDT(θ_c)	$w(0)$	0.0032	0.0192	0.0760	1.8918	7.5662
FSDT(TM)	$w(0)$	0.0032	0.0192	0.0760	1.8918	7.5662
CLT(θ_a)	$w(0)$	0.0018	0.0111	0.0443	1.1073	4.4291
CLT(θ_c)	$w(0)$	0.0032	0.0192	0.0760	1.8918	7.5662
CLT(TM)	$w(0)$	0.0032	0.0192	0.0760	1.8918	7.5662

Table 4
Two-layered isotropic plate with sovra-temperature applied on its top and bottom surfaces. Displacement u in [mm] for several two-dimensional theories and thickness ratios.

	a/h	2	5	10	50	100
LD4(θ_a)	$u(h/2)$	−0.0044	−0.0091	−0.0176	−0.0868	−0.1735
LD4(θ_c)	$u(h/2)$	−0.0035	−0.0077	−0.0151	−0.0748	−0.1496
LD4(TM)	$u(h/2)$	−0.0032	−0.0076	−0.0150	−0.0748	−0.1496
ED4(θ_a)	$u(h/2)$	−0.0043	−0.0091	−0.0175	−0.0866	−0.1732
ED4(θ_c)	$u(h/2)$	−0.0035	−0.0077	−0.0151	−0.0748	−0.1495
ED4(TM)	$u(h/2)$	−0.0032	−0.0076	−0.0150	−0.0748	−0.1495
LD2(θ_a)	$u(h/2)$	−0.0044	−0.0091	−0.0176	−0.0868	−0.1735
LD2(θ_c)	$u(h/2)$	−0.0033	−0.0076	−0.0150	−0.0748	−0.1496
LD2(TM)	$u(h/2)$	−0.0033	−0.0076	−0.0150	−0.0748	−0.1496
FSDT(θ_a)	$u(h/2)$	−0.0051	−0.0127	−0.0253	−0.1268	−0.2535
FSDT(θ_c)	$u(h/2)$	−0.0042	−0.0108	−0.0218	−0.1091	−0.2182
FSDT(TM)	$u(h/2)$	−0.0042	−0.0108	−0.0218	−0.1091	−0.2182
CLT(θ_a)	$u(h/2)$	−0.0051	−0.0127	−0.0253	−0.1268	−0.2535
CLT(θ_c)	$u(h/2)$	−0.0042	−0.0108	−0.0218	−0.1091	−0.2182
CLT(TM)	$u(h/2)$	−0.0042	−0.0108	−0.0218	−0.1091	−0.2182

Table 5
Two-layered composite plate (0°/90°) with sovra-temperature applied on its top and bottom surfaces. Displacement w in [mm] for several two-dimensional theories and thickness ratios.

	a/h	2	5	10	50	100
LD4(θ_a)	$w(0)$	0.0014	0.0141	0.0587	1.4857	5.9448
LD4(θ_c)	$w(0)$	0.0009	0.0137	0.0585	1.4855	5.9446
LD4(TM)	$w(0)$	0.0012	0.0116	0.0553	1.4818	5.9409
ED4(θ_a)	$w(0)$	0.0014	0.0141	0.0588	1.4857	5.9446
ED4(θ_c)	$w(0)$	0.0008	0.0137	0.0585	1.4855	5.9444
ED4(TM)	$w(0)$	0.0012	0.0117	0.0553	1.4818	5.9407
LD2(θ_a)	$w(0)$	0.0010	0.0135	0.0581	1.4850	5.9441
LD2(θ_c)	$w(0)$	0.0014	0.0115	0.0549	1.4813	5.9404
LD2(TM)	$w(0)$	0.0015	0.0114	0.0549	1.4813	5.9404
FSDT(θ_a)	$w(0)$	0.0031	0.0192	0.0769	1.9234	7.6937
FSDT(θ_c)	$w(0)$	0.0031	0.0192	0.0769	1.9234	7.6937
FSDT(TM)	$w(0)$	0.0031	0.0192	0.0769	1.9234	7.6937
CLT(θ_a)	$w(0)$	0.0031	0.0192	0.0769	1.9234	7.6937
CLT(θ_c)	$w(0)$	0.0031	0.0192	0.0769	1.9234	7.6937
CLT(TM)	$w(0)$	0.0031	0.0192	0.0769	1.9234	7.6937

partially coupled models with calculated temperature profiles (θ_c) and the fully coupled models (TM) are always coincident, but the solution of Fourier's heat conduction equation is difficult for very thick plates ($a/h = 2$, as illustrated in Fig. 4): Fourier's heat conduction equation is solved by using a solution which is a combination of an hyperbolic sine and an hyperbolic cosine (see [14]). This type of solution strongly depends on the thickness of the plate and it does not properly work for very thick plates. In conclusion, the fully coupled models are a valid alternative to partially coupled models with calculated temperature profile θ_c: they give the same results, but in a simpler way (without solving the Fourier equation, but directly obtaining both displacements and temperature from the governing equation).

A two-layered isotropic plate is considered in Tables 3 and 4, and in Fig. 5. The partially coupled models, with assumed temperature profile (θ_a), give large errors for both thick and thin plates. In fact, as suggested in Fig. 5, the temperature profile is never linear, even when the plate is thin: the two layers have different conductivity coefficients and this means linear temperature profiles in each layer but with different slopes. As in the one-layered case, partially coupled models with a calculated temperature profile (θ_c) and fully coupled models are coincident. The plate is two-layered with a strong transverse anisotropy, therefore the importance

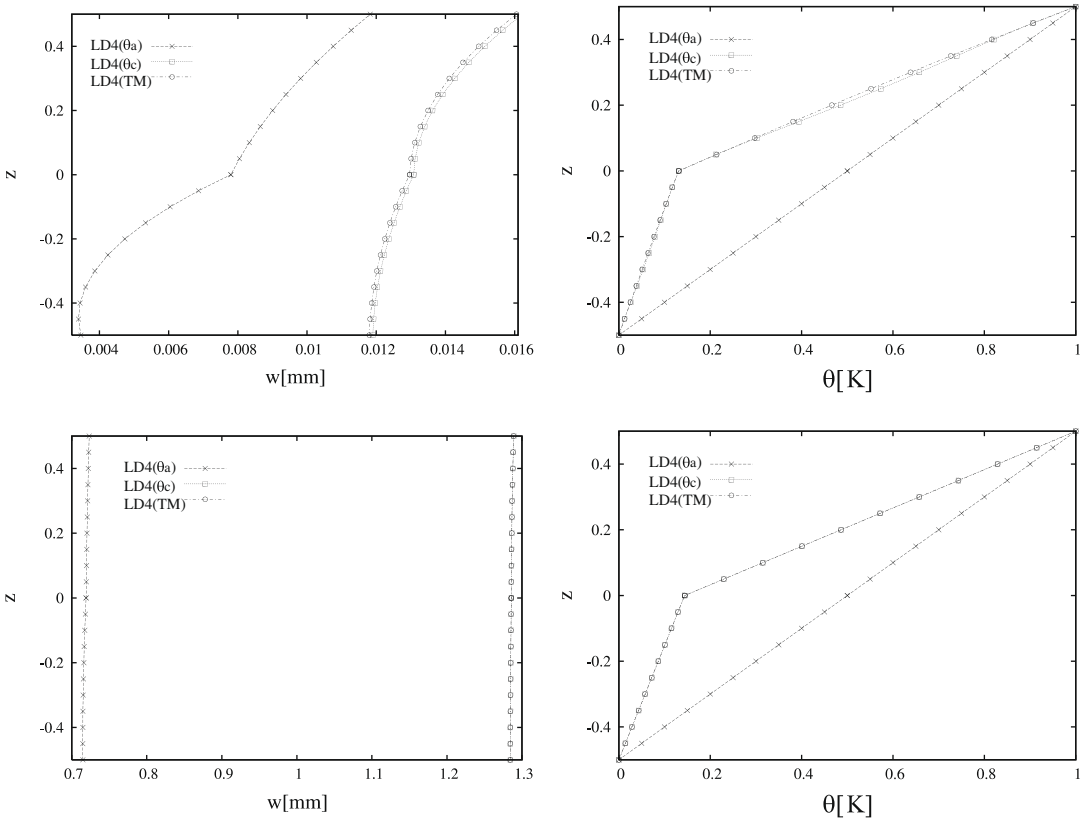

Fig. 5. Two-layered isotropic plate with sovra-temperature applied on its top and bottom surfaces. Displacement w and sovra-temperature θ vs. z for $a/h = 5, 50$ (top and bottom figures, respectively).

Table 6
Two-layered composite plate (0°/90°) with sovra-temperature applied on its top and bottom surfaces. Displacement u in [mm] for several two-dimensional theories and thickness ratios.

	a/h	2	5	10	50	100
LD4(θ_a)	$u(h/2)$	−0.0136	−0.0171	−0.0225	−0.0882	−0.1747
LD4(θ_c)	$u(h/2)$	−0.0092	−0.0144	−0.0213	−0.0880	−0.1746
LD4(TM)	$u(h/2)$	−0.0053	−0.0117	−0.0200	−0.0878	−0.1745
ED4(θ_a)	$u(h/2)$	−0.0135	−0.0168	−0.0223	−0.0881	−0.1747
ED4(θ_c)	$u(h/2)$	−0.0091	−0.0142	−0.0211	−0.0879	−0.1746
ED4(TM)	$u(h/2)$	−0.0053	−0.0116	−0.0198	−0.0877	−0.1745
LD2(θ_a)	$u(h/2)$	−0.0134	−0.0169	−0.0223	−0.0881	−0.1747
LD2(θ_c)	$u(h/2)$	−0.0064	−0.0118	−0.0199	−0.0877	−0.1745
LD2(TM)	$u(h/2)$	−0.0062	−0.0118	−0.0199	−0.0877	−0.1745
FSDT(θ_a)	$u(h/2)$	−0.0084	−0.0155	−0.0254	−0.1136	−0.2262
FSDT(θ_c)	$u(h/2)$	−0.0061	−0.0132	−0.0241	−0.1133	−0.2261
FSDT(TM)	$u(h/2)$	−0.0053	−0.0129	−0.0241	−0.1133	−0.2262
CLT(θ_a)	$u(h/2)$	−0.0045	−0.0113	−0.0226	−0.1129	−0.2259
CLT(θ_c)	$u(h/2)$	−0.0041	−0.0105	−0.0218	−0.1127	−0.2258
CLT(TM)	$u(h/2)$	−0.0039	−0.0103	−0.0218	−0.1127	−0.2258

Table 7
One-layered isotropic plate with mechanical load $p_z = -200{,}000$ Pa applied at the top. Displacements u and w in [mm] for several two-dimensional theories and thickness ratios.

	a/h	2	5	10	50	100
		($\times 10^{-1}$)				
LD4(TM)	$w(0)$	−0.0263	−0.0570	−0.7988	−476.35	−7610.0
LD4	$w(0)$	−0.0265	−0.0575	−0.8062	−480.86	−7682.2
LD4(TM)	$u(h/2)$	0.0093	0.0145	0.1186	14.930	119.47
LD4	$u(h/2)$	0.0095	0.0147	0.1197	15.072	120.60
LD2(TM)	$w(0)$	−0.0245	−0.0557	−0.7937	−476.22	−7609.5
LD2	$w(0)$	−0.0246	−0.0562	−0.8010	−480.73	−7681.7
LD2(TM)	$u(h/2)$	0.0073	0.0141	0.1177	14.926	119.46
LD2	$u(h/2)$	0.0075	0.0143	0.1189	15.068	120.59
FSDT(TM)	$w(0)$	−0.0265	−0.0561	−0.7895	−471.78	−7537.7
FSDT	$w(0)$	−0.0267	−0.0570	−0.8039	−480.80	−7682.0
FSDT(TM)	$u(h/2)$	0.0095	0.0148	0.1183	14.793	118.34
FSDT	$u(h/2)$	0.0096	0.0151	0.1206	15.076	120.61
CLT(TM)	$w(0)$	−0.0120	−0.0471	−0.7534	−470.88	−7534.1
CLT	$w(0)$	−0.0123	−0.0480	−0.7678	−479.90	−7678.4
CLT(TM)	$u(h/2)$	0.0095	0.0148	0.1183	14.793	118.34
CLT	$u(h/2)$	0.0096	0.0151	0.1206	15.076	120.61

of the kinematics for the displacements approximation can clearly be noticed in Tables 3 and 4 and in Fig. 5: LW theories are preferred to ESL theories. Classical theories, such as CLT and FSDT, are inadequate for each proposed thermo-mechanical model.

The last case concerns the two-layered composite plate. Transverse displacement w in the middle of the plate and in-plane displacement u at the top are given in Tables 5 and 6, respectively. Fig. 6 shows transverse displacement and temperature in the thickness direction z for thick and thin plates. The two layers are made of the same material (carbon fibre reinforced layers), the only difference is the fibre orientation (0° for the bottom layer and 90° for the top layer). This means that the conductivity coefficient κ_{33} is the same for both layers, and the in-plane coefficients κ_{11} and κ_{22} are exchanged in the two layers (the plate is square and this does not represent a difference). Therefore, the temperature profiles in Fig. 6 are easily explained: there is no change in slope in the two layers, and the profile is linear for thin plates. Fig. 6 explains the results in Tables 5 and 6: for thin and moderately thin plates, θ_a, θ_c and *TM* models give very similar results, even thought the *TM* models appear more efficient than the partially coupled models. However, transverse anisotropy, in terms of

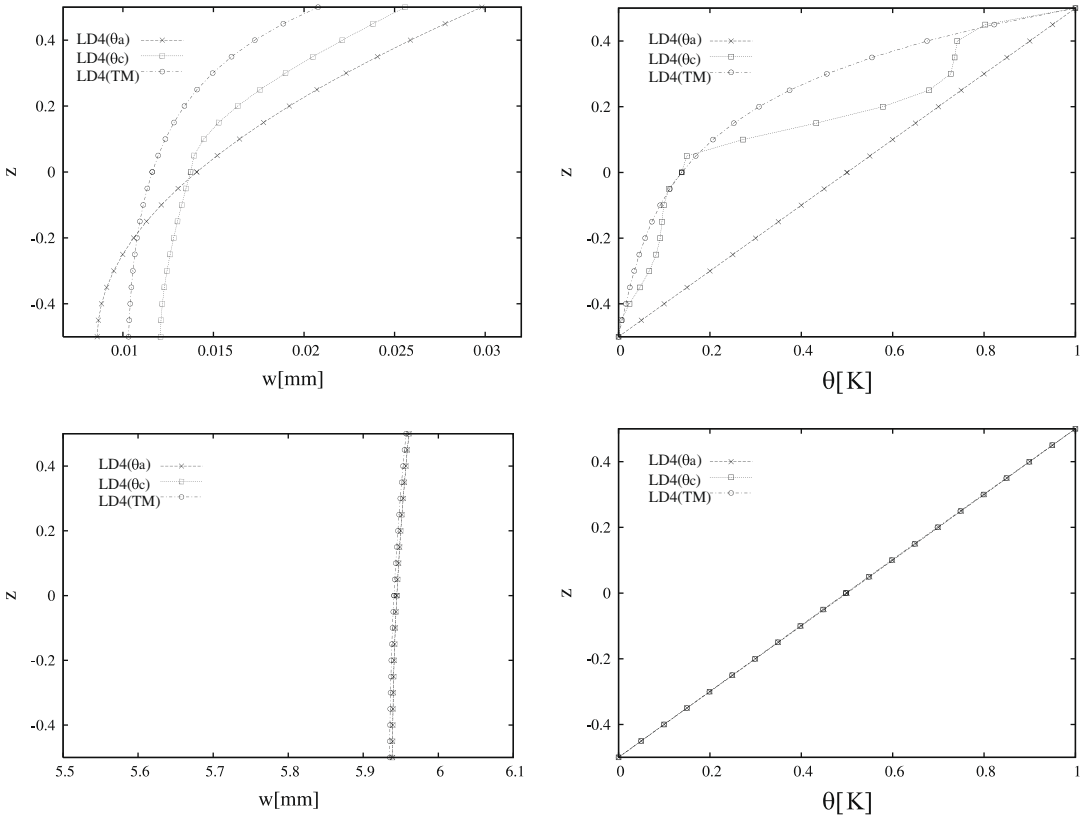

Fig. 6. Two-layered composite plate (0°/90°) with sovra-temperature applied on its top and bottom surfaces. Displacement w and sovra-temperature θ vs. z for $a/h = 5, 100$ (top and bottom figures, respectively).

Table 8
Two-layered isotropic plate with mechanical load $p_z = -200{,}000$ Pa applied at the top. Displacements u and w in [mm] for several two-dimensional theories and thickness ratios.

	a/h	2	5	10	50	100
		($\times 10^{-1}$)				
LD4(TM)	$w(0)$	−0.0220	−0.0471	−0.6567	−391.01	−6246.3
LD4	$w(0)$	−0.0221	−0.0473	−0.6605	−393.36	−6284.0
LD4(TM)	$u(h/2)$	0.0073	0.0109	0.0877	11.000	880.06
LD4	$u(h/2)$	0.0074	0.0109	0.0881	11.044	883.57
ED4(TM)	$w(0)$	−0.0218	−0.0470	−0.6564	−390.99	−6246.3
ED4	$w(0)$	−0.0219	−0.0472	−0.6601	−393.35	−6283.9
ED4(TM)	$u(h/2)$	0.0073	0.0109	0.0877	11.000	880.06
ED4	$u(h/2)$	0.0073	0.0109	0.0881	11.043	883.57
LD2(TM)	$w(0)$	−0.0218	−0.0470	−0.6564	−391.00	−6246.3
LD2	$w(0)$	−0.0218	−0.0472	−0.6602	−393.35	−6284.0
LD2(TM)	$u(h/2)$	0.0071	0.0109	0.0877	10.999	880.05
LD2	$u(h/2)$	0.0072	0.0109	0.0881	11.043	883.57
FSDT(TM)	$w(0)$	−0.0215	−0.0460	−0.6495	−388.52	−6207.6
FSDT	$w(0)$	−0.0217	−0.0465	−0.6571	−393.27	−6283.7
FSDT(TM)	$u(h/2)$	0.0070	0.0109	0.0876	10.955	876.41
FSDT	$u(h/2)$	0.0071	0.0110	0.0884	11.045	883.60
CLT(TM)	$w(0)$	−0.0099	−0.0388	−0.6205	−387.80	−6204.7
CLT	$w(0)$	−0.0100	−0.0392	−0.6581	−392.55	−6280.8
CLT(TM)	$u(h/2)$	0.0070	0.0109	0.0876	10.955	876.41
CLT	$u(h/2)$	0.0071	0.0110	0.0884	11.045	883.60

elastic properties, remains, therefore the importance of higher orders of expansion for the displacement can be noted and the inadequacy of CLT and FSDT is confirmed. As in the first case, the solution of the Fourier heat conduction equation is difficult for thick plates ($a/h = 5$ in Fig. 6).

For all the three proposed cases, the fully coupled models appear to be the best solution: they give the same results as the partially coupled θ_c models, but both the displacements and temperature are directly obtained from the governing equations. On the contrary, in the θ_c model, the temperature profile must be a priori calculated, by solving the Fourier heat conduction equation, and then introduced into the governing equation as an external load.

7.2. Applied mechanical load

The considered plates are subjected to a mechanical load applied at the top in the z direction, with amplitude $p_z = -200{,}000$ Pa and harmonic distribution in the plane (waves number $m = n = 1$). A comparison is made between the pure mechanical models (see Eq. (51), with inertial contribution and thermal load discarded) and the fully coupled models (TM) (see Eq. (65), with inertial contribution and thermal load discarded). In general, when a model considers thermo-mechanical coupling, smaller displacements are obtained and a temperature profile in the thickness direction is originated.

The first case considers a one-layered isotropic plate, as in [26]. Transverse and in-plane displacements are given for the pure mechanical models and for the fully coupled thermo-mechanical models in Table 7. The pure mechanical models give larger displacements than the fully coupled models; in the latter, the deformation field produces a change in temperature in the considered body. The differences in displacements, as suggested in Nowinski's book [1] and then confirmed in Carrera et al. [26], is less than 1% for each thickness ratio and each proposed two-dimensional theory. In this case, classical theories, such as CLT and FSDT, give correct results for thin plates, because the plate is isotropic and one-layered, but if thermo-mechanical coupling is accounted for, they do not work properly because their degrees of freedom are

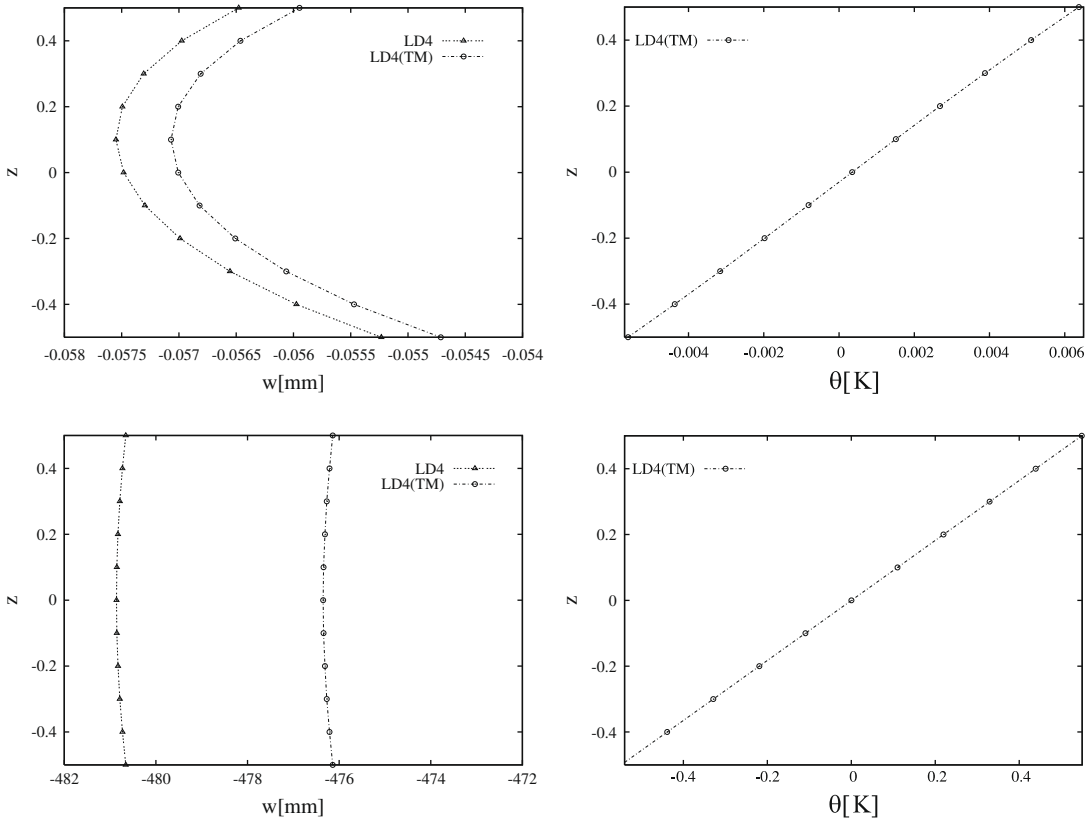

Fig. 7. One-layered isotropic plate with mechanical load $p_z = -200{,}000$ Pa applied at the top. Displacement w and sovra-temperature θ vs. z for $a/h = 5, 50$ (top and bottom figures, respectively).

Table 9
Two-layered composite plate (0°/90°) with mechanical load $p_z = -200{,}000$ Pa applied at the top. Displacements u and w in [mm] for several two-dimensional theories and thickness ratios.

	a/h	2	5	10	50	100
LD4(TM)	$w(0)$	−0.0224	−0.3098	3.5531	−1935.7	−30,828
LD4	$w(0)$	−0.0224	−0.3099	3.5547	−1936.6	−30,843
LD4(TM)	$u(h/2)$	0.0078	0.0956	0.7268	88.962	711.19
LD4	$u(h/2)$	0.0078	0.0957	0.7272	89.006	711.54
ED4(TM)	$w(0)$	−0.0215	−0.3050	−3.5343	−1935.2	−30,826
ED4	$w(0)$	−0.0215	−0.3051	−3.5359	−1936.1	−30,840
ED4(TM)	$u(h/2)$	0.0076	0.0954	0.7260	88.954	711.15
ED4	$u(h/2)$	0.0077	0.0954	0.7264	88.999	711.51
LD2(TM)	$w(0)$	−0.0210	−0.3007	−3.5158	−1934.8	−30,825
LD2	$w(0)$	−0.0210	−0.3008	−3.5173	−1935.7	−30,839
LD2(TM)	$u(h/2)$	0.0071	0.0923	0.7186	88.918	711.10
LD2	$u(h/2)$	0.0071	0.0923	0.7191	88.963	711.46
FSDT(TM)	$w(0)$	−0.0217	−0.2972	−3.4966	−1933.7	−30,813
FSDT	$w(0)$	−0.0217	−0.2974	−3.4991	−1935.2	−30,837
FSDT(TM)	$u(h/2)$	0.0057	0.0888	0.7108	88.849	710.79
FSDT	$u(h/2)$	0.0057	0.0889	0.7114	88.922	711.38
CLT(TM)	$w(0)$	−0.0049	−0.1923	−3.0771	−1923.2	−30,771
CLT	$w(0)$	−0.0049	−0.1925	−3.0796	−1924.7	−30,796
CLT(TM)	$u(h/2)$	0.0057	0.0888	0.7108	88.849	710.79
CLT	$u(h/2)$	0.0057	0.0889	0.7114	88.922	711.38

not sufficient to accurately include the thermal part. LD4 and LD4(TM) models are compared in Fig. 7, in terms of transverse displacement, for a thick and a moderately thin plate. Through the thickness z, the transverse displacement obtained with the pure mechanical model is always larger than that obtained with the fully coupled model. This happens because, when a mechanical load is applied, a small part of the work done by this load, is used to develop an increment in temperature (the maximum value is about 0.006 K for a thick plate and about 0.5 K for a thin plate). The temperature values are remarkably small because of the small coupling effect between the thermal and mechanical fields. The bending problem, as described in Fig. 7, leads to an increment in temperature for the compressed part of the plate and a decrease in temperature for the enlarged part of the plate.

The case of the two-layered isotropic plate has been investigated in Table 8 and in Fig. 8. The differences in displacements are small, as for the one-layered case: less than 1% for both displacement components, and for each thickness ratio and each proposed two-dimensional theory. This small coupling effect is also confirmed in Fig. 8, where maximum increments in temperature, of about 0.003 K and about 0.2 K, are obtained for thick and moderately thin plates, respectively. The two layers have different thermal properties, therefore the obtained temperature profiles have different slopes in the two considered layers (see Fig. 8). The transverse anisotropy, in terms of elastic properties, shows the importance of higher orders of expansion and the inadequacy of CLT and FSDT theories.

The results for the two-layered composite plate are given in Table 9 and in Fig. 9. The small coupling effect is here confirmed by the differences in terms of displacements (less than 0.5%) and the maximum increment in temperature (about 0.02 K for the thick plate and about 1 K for the thin plate). According to these results, the coupling effect in composite materials seems less pronounced than those in isotropic metallic materials. The temperature profiles, given in Fig. 9, have a less marked zigzag form than the two-layered isotropic plate, because the thermal expansion coefficient α_3 is the same for the two layers, and only the α_1 and α_2 coefficients are exchanged in the two layers. The importance

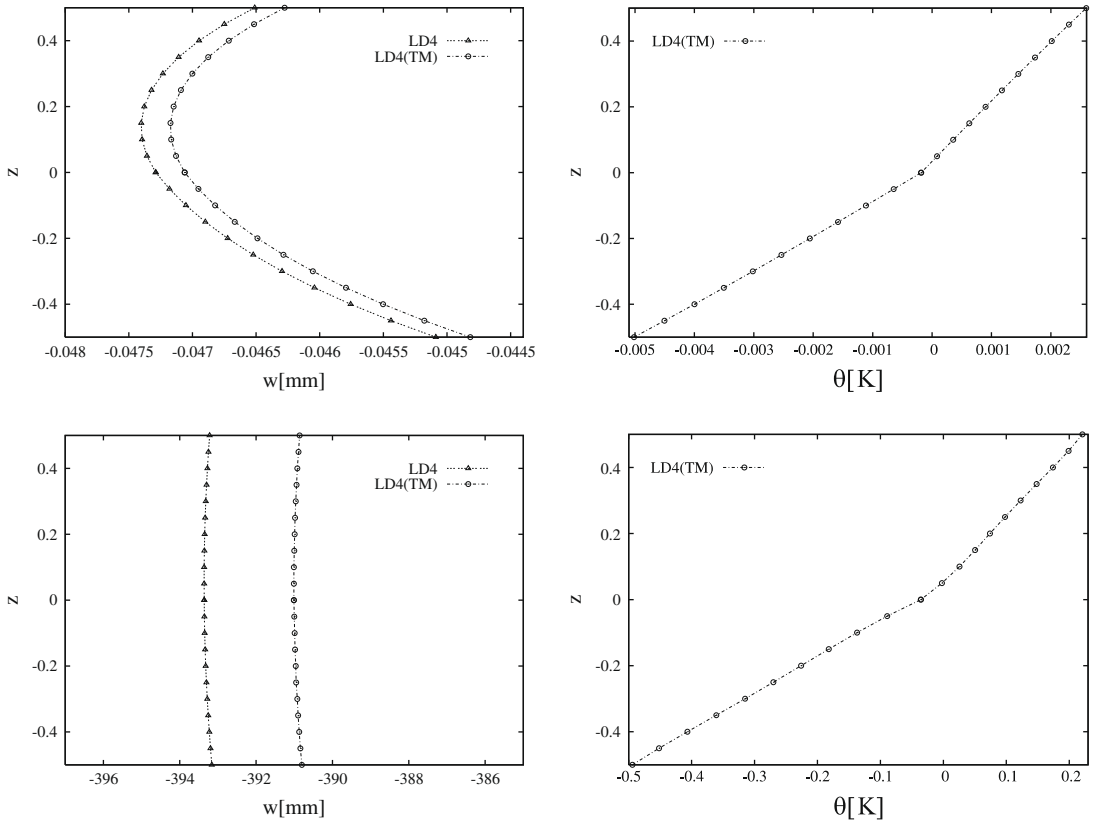

Fig. 8. Two-layered isotropic plate with mechanical load $p_z = -200{,}000$ Pa applied at the top. Displacement w and sovra-temperature θ vs. z for $a/h = 5, 50$ (top and bottom figures, respectively).

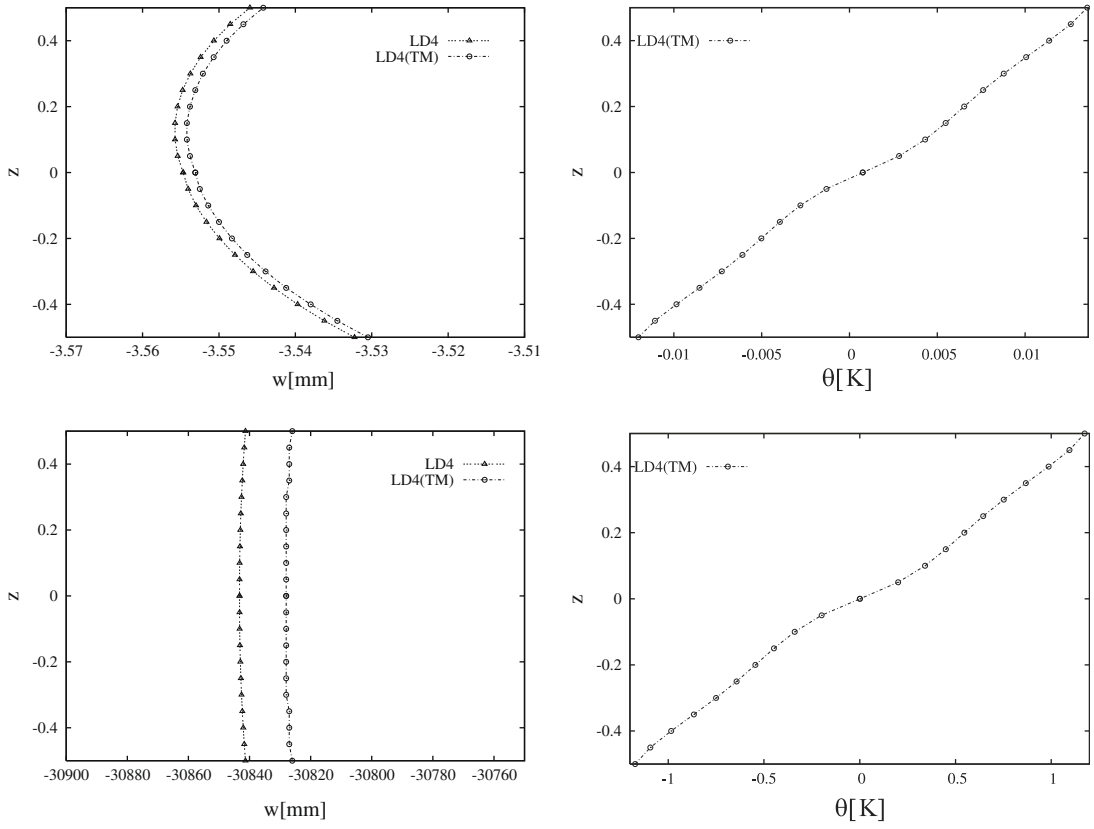

Fig. 9. Two-layered composite plate (0°/90°) with mechanical load $p_z = -200{,}000$ Pa applied at the top. Displacement w and sovra-temperature θ vs. z for $a/h = 10, 100$ (top and bottom figures, respectively).

Table 10
One-layered isotropic plate, free vibrations problem. Fundamental frequency f in Hz for several two-dimensional theories and thickness ratios. Wave numbers $m = n = 1$. The full coupling problem is indicated with (TM)* in case of imposed temperature conditions and (TM) in case of free temperature conditions.

a/h	2	5	10	50	100
LD4(TM)	766.03	173.10	47.158	1.9481	0.4875
LD4(TM)*	765.32	172.88	47.094	1.9454	0.4869
LD4	763.94	172.40	46.946	1.9390	0.4852
LD2(TM)	788.72	174.86	47.306	1.9484	0.4876
LD2(TM)*	786.64	174.15	47.093	1.9392	0.4853
LD2	786.64	174.15	47.093	1.9392	0.4853
FSDT(TM)	790.02	175.52	47.517	1.9577	0.4899
FSDT	786.06	174.10	47.088	1.9392	0.4853
CLT(TM)	1031.3	189.87	48.607	1.9596	0.4900
CLT	1021.5	188.08	48.148	1.9411	0.4854

Table 11
Two-layered isotropic plate, free vibrations problem. Fundamental frequency f in Hz for several two-dimensional theories and thickness ratios. Wave numbers $m = n = 1$. The full coupling problem is indicated with (TM)* in case of imposed temperature conditions and (TM) in case of free temperature conditions.

a/h	2	5	10	50	100
LD4(TM)	744.80	168.31	46.847	1.8938	0.4739
LD4(TM)*	744.65	168.26	46.832	1.8931	0.4738
LD4	743.64	167.89	45.716	1.8831	0.4725
ED4(TM)	746.71	168.46	45.860	1.8938	0.4739
ED4(TM)*	746.55	168.41	45.845	1.8932	0.4738
ED4	745.53	168.04	45.729	1.8881	0.4725
LD2(TM)	747.35	168.44	45.857	1.8938	0.4739
LD2(TM)*	746.82	168.29	45.812	1.8919	0.4735
LD2	746.18	168.02	45.726	1.8881	0.4725
FSDT(TM)	772.12	170.76	46.149	1.8999	0.4754
FSDT	769.53	169.87	45.881	1.8884	0.4725
CLT(TM)	1098.8	184.48	47.185	1.9017	0.4755
CLT	1098.8	183.36	46.899	1.8902	0.4726

of LW models and higher orders of expansion is clearly shown in Table 9.

In conclusion, the thermo-mechanical coupling effect is very small in the considered plates and can be discarded. However, fully coupled thermo-mechanical models could be used for future applications, such as thermography investigations [51–53]: the increment in temperature is experimentally measured to determine the strains and stresses which have generated it.

7.3. Free vibrations analysis

Free vibration analysis is investigated for the three proposed simply supported plates. Imposing the wave numbers ($m = n = 1$) in the plane, results are given in terms of fundamental frequency f in Hz. In this dynamic case, the pure mechanical models give smaller frequencies than those obtained with the fully coupled thermo-mechanical models. Table 10 gives the fundamental frequencies for a one-layered isotropic plate, Table 11 for a two-layered isotropic plate, and finally, Table 12 presents results for a two-layered composite plate. The pure mechanical model uses the governing Eq. (51) and discards the thermal and mechanical loads, while the fully coupled thermo-mechanical model considers the governing Eq. (65) by discarding the thermal and mechanical loads. In the case of fully coupled models, the external surfaces of the plate can have imposed conditions on the sovra-temperature

Table 12
Two-layered composite plate (0°/90°), free vibrations problem. Fundamental frequency f in Hz for several two-dimensional theories and thickness ratios. Wave numbers $m = n = 1$. The full coupling problem is indicated with (TM)* in case of imposed temperature conditions and (TM) in case of free temperature conditions.

a/h	2	5	10	50	100
LD4(TM)	324.40	89.369	26.780	1.1608	0.2910
LD4(TM)*	324.39	89.367	26.799	1.1608	0.2910
LD4	324.36	89.352	26.794	1.1605	0.2909
ED4(TM)	329.08	89.994	26.868	1.1610	0.2910
ED4(TM)*	329.08	89.993	26.868	1.1609	0.2910
ED4	329.04	89.978	26.863	1.1607	0.2909
LD2(TM)	333.30	90.686	26.940	1.1611	0.2910
LD2(TM)*	333.29	90.680	26.938	1.1610	0.2910
LD2	333.27	90.670	26.934	1.1608	0.2904
FSDT(TM)	340.30	91.593	27.041	1.1615	0.2911
FSDT	340.00	91.568	27.032	1.1610	0.2910
CLT(TM)	555.69	110.57	28.740	1.1646	0.2913
CLT	555.47	110.52	28.728	1.1642	0.2912

($\theta_t = \theta_b = 0$, which means the temperature on the external surfaces equals the external room temperature), or no conditions on the sovra-temperature are applied. The first case is here indicated as (TM)*, the second as (TM).

The differences in Table 10 between the pure mechanical fundamental frequency and the fully coupled fundamental frequency are less than 1.0% for each investigated thickness ratio and for each proposed two-dimensional theory. The frequencies obtained with the thermo-mechanical models are larger because, when the thermal effect is included, the rigidity matrix undergoes a sort of increase in rigidity. Frequencies obtained with the thermo-mechanical models with imposed thermal conditions (TM)* are smaller than those obtained with free thermal conditions (TM). For classical theories, such as CLT and FSDT, the (TM)* case cannot be considered, because the employed degrees of freedom are not sufficient to impose such conditions. Fundamental frequency modes, are given in Fig. 10 for both free and imposed thermal conditions, in terms of displacements and temperature, for a thick plate. The first mode is a bending mode, therefore the temperature increases in the compressed part and decreases in the enlarged part of the plate; when the imposed thermal conditions are considered, the sovra-temperature is zero at the top and bottom of the plate. The values given by the modes have only a qualitative sense and they are normalized with the maximum values.

Table 11 proposes the same results as Table 10, but for a two-layered plate. The same conclusions can be drawn. However the importance of refined theories is clearly indicated for thick plates. The modes, in terms of displacement and temperature, are given in Fig. 11 for a thick plate ($a/h = 5$); in this case, the mode in terms of temperature is not linear, even though a bending mode, in terms of displacements, is considered.

A two-layered composite plate is investigated in Table 12 and in Fig. 12; the coupling effect is less pronounced than in the other two cases and it disappears for very thin plates. The modes plotted in Fig. 12 are for a moderately thin plate ($a/h = 50$). In order to obtain correct values of frequencies for thick plates, higher orders of expansion are necessary.

In conclusion, for the free vibration analysis, the thermo-mechanical coupling effect is very small and it can be discarded. However, fully coupled models are very interesting because they give the modes in terms of displacements and temperature. A possible application could be thermography investigations, as suggested in [51–53].

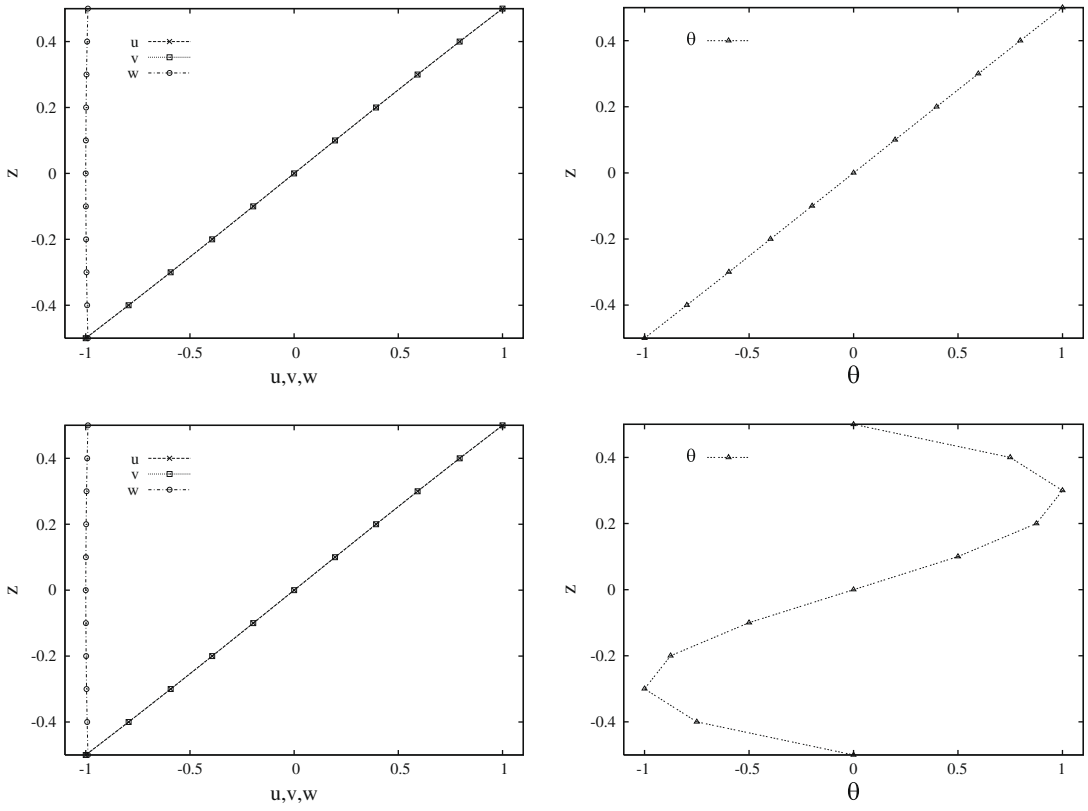

Fig. 10. One-layered isotropic plate, free vibrations problem. Modes in term of displacements and sovra-temperature for the fundamental frequency: $m = n = 1$ and $a/h = 10$. LD4 theory for free temperature conditions (top figures) and imposed temperature conditions (bottom figures).

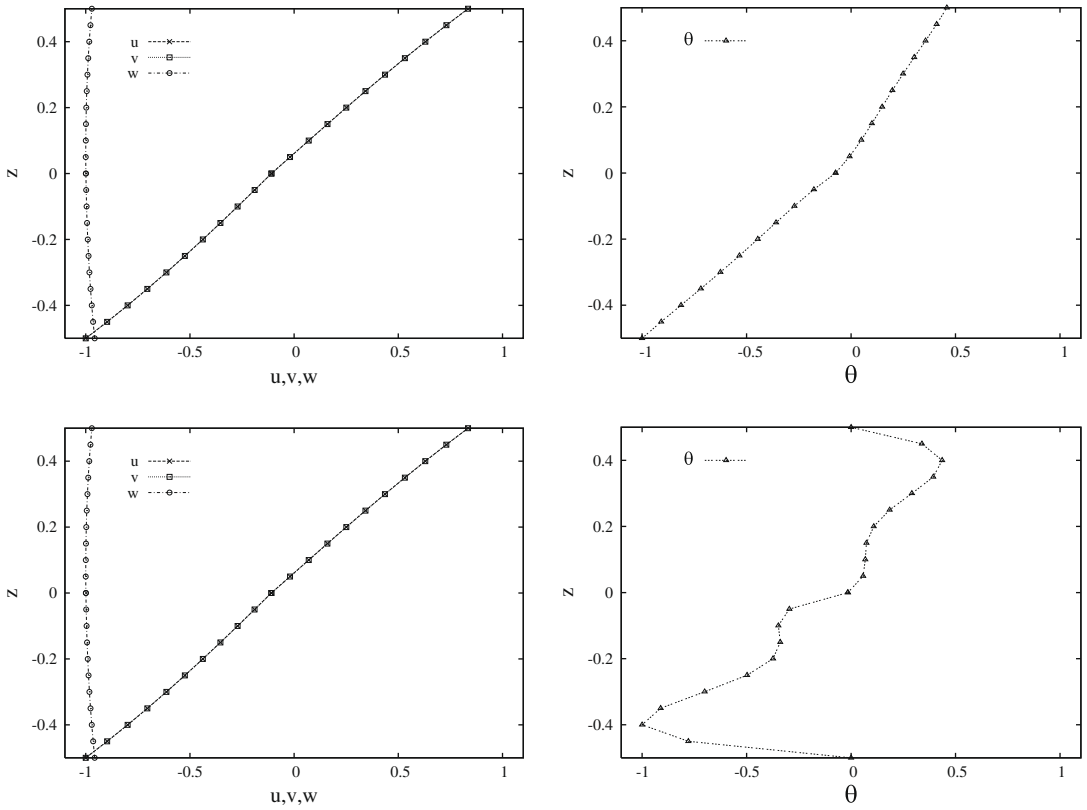

Fig. 11. Two-layered isotropic plate, free vibrations problem. Modes in term of displacements and sovra-temperature for the fundamental frequency: $m = n = 1$ and $a/h = 5$. LD4 theory for free temperature conditions (top figures) and imposed temperature conditions (bottom figures).

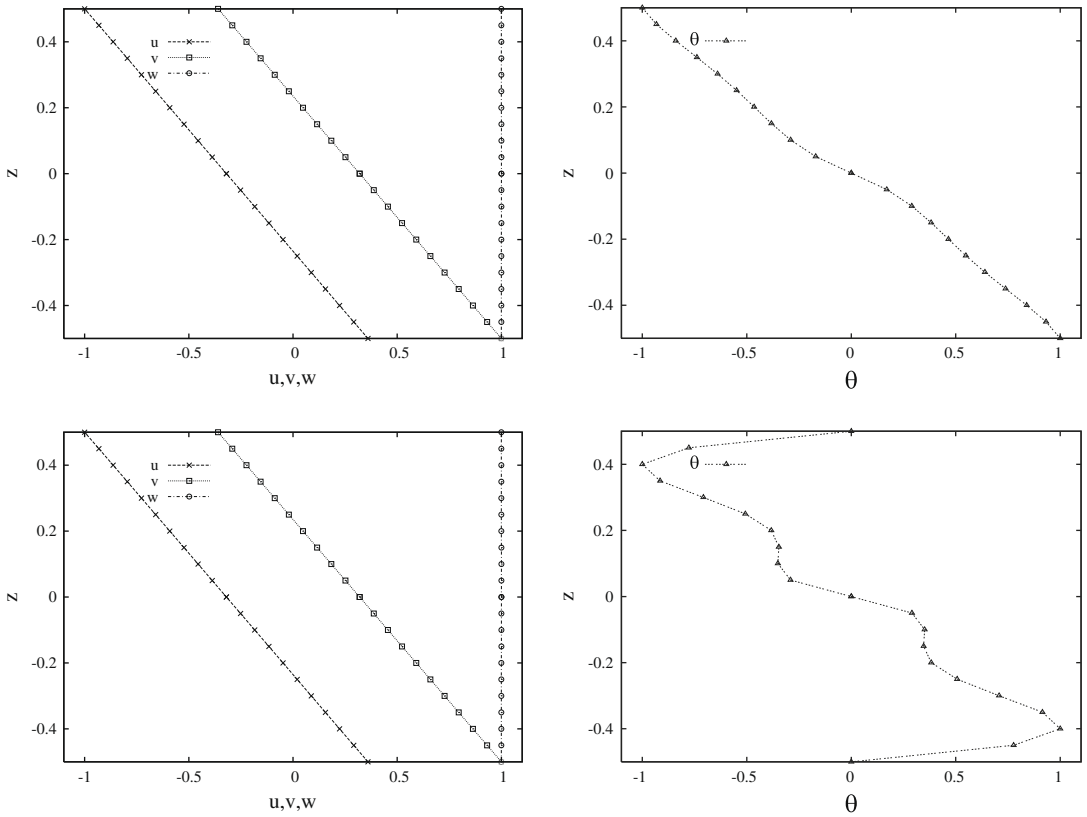

Fig. 12. Two-layered composite plate (0°/90°), free vibrations problem. Modes in term of displacements and sovra-temperature for the fundamental frequency: $m = n = 1$ and $a/h = 50$. LD4 theory for free temperature conditions (top figures) and imposed temperature conditions (bottom figures).

8. Conclusions

A fully coupled thermo-mechanical analysis has been discussed in this paper. Both displacements and temperature are considered as primary variables of the problem, and they can be directly obtained from the solution of the governing equations. These features lead to some advantages:

- In the case of a temperature applied to the external surfaces of the plate, the fully coupled analysis permits such values to be easily imposed in the governing equations, and the relative displacements and temperature profile are directly obtained from the solutions of such equations. The advantages, with respect to a partially coupled thermo-mechanical analysis, have been clearly indicated. In this latter case, in fact, the temperature profile must be a priori defined (assuming it linear in the thickness direction or calculating it by solving the Fourier heat conduction equation) to determine the thermal load.
- In the case of a mechanical load applied to the structure, the fully coupled thermo-mechanical analysis permits the displacement and the temperature generated by the strains to be evaluated. The effect of the thermo-mechanical coupling has been evaluated through comparisons with pure mechanical analysis. The coupling effect is very small and it can therefore be discarded in such an analysis. However, thermo-mechanical coupling could be used for thermography investigations.
- The effect of the thermo-mechanical coupling has also been evaluated for free vibration analysis; the fully coupled thermo-mechanical analysis permits the frequency values and the vibration modes to be evaluated in terms of the displacement and temperature. The effect of thermo-mechanical coupling has also been evaluated for the dynamic case through comparisons with pure mechanical analysis. The coupling effect is very small and it can therefore be discarded in a free vibration analysis. However, thermo-mechanical coupling could be used for thermography investigations, as already suggested for the static case.

Future works will extend the present formulation to shell geometries. In addition, the effect of the time evolution of the heat flux could be added, in the relaxation term, in order to analyze the transient regime of the proposed cases.

References

[1] Nowinski JL. Theory of thermoelasticity with applications. The Netherlands: Sijthoff & Noordhoff; 1978.
[2] Librescu L, Marzocca P. Thermal stresses'03, vol. 1. Blacksburg (VA, USA): Virginia Polytechnic Institute and State University; 2003.
[3] Librescu L, Marzocca P. Thermal stresses'03, Vol. 2. Blacksburg (VA, USA): Virginia Polytechnic Institute and State University; 2003.
[4] Noor AK, Burton WS. Computational models for high-temperature multilayered composite plates and shells. Appl Mech Rev 1992;45(10):419–46.
[5] Wu Z, Chen W. A global–local higher order theory for multilayered shells and the analysis of laminated cylindrical shell panels. Compos Struct 2008;84(4):350–61.
[6] Brischetto S, Carrera E. Thermal stress analysis by refined multilayered composite shell theories. J Thermal Stress 2009;32(1):165–86.
[7] Bhaskar K, Varadan TK, Ali JSM. Thermoelastic solution for orthotropic and anisotropic composite laminates. Compos Part B: Eng 1996;27(5):415–20.
[8] Khare RK, Kant T, Garg AK. Closed-form thermo-mechanical solutions of higher-order theories of cross-ply laminated shallow shells. Compos Struct 2003;59(3):313–40.
[9] Khdeir AA. Thermoelastic analysis of cross-ply laminated circular cylindrical shells. Int J Solids Struct 1996;33(27):4007–17.
[10] Birsan M. Thermal stresses in cylindrical Cosserat elastic shells. Eur J Mech – A/Solids 2009;28(1):94–101.
[11] Carrera E. An assessment of mixed and classical theories for the thermal stress analysis of orthotropic multilayered plates. J Thermal Stress 2000;23(9):797–831.
[12] Carrera E. Temperature profile influence on layered plates response considering classical and advanced theories. AIAA J 2002;40(9):1885–96.
[13] Rolfes R, Noack J, Taeschner M. High performance 3D-analysis of thermo-mechanically loaded composite structures. Compos Struct 1999;46(4):367–79.
[14] Brischetto S. Effect of the through-the-thickness temperature distribution on the response of layered and composite shells. Int J Appl Mech 2009;1(4):1–25.
[15] Brischetto S, Leetsch R, Carrera E, Wallmersperger T, Kröplin B. Thermo-mechanical bending of functionally graded plates. J Thermal Stress 2008;31(3):286–308.
[16] Altay GA, Dökmeci MC. Some variational principles for linear coupled thermoelasticity. Int J Solids Struct 1996;33(26):3937–48.
[17] Altay GA, Dökmeci MC. Fundamental variational equations of discontinuous thermopiezoelectric fields. Int J Eng Sci 1996;34(7):769–82.
[18] Das NC, Das SN, Das B. Eigenvalue approach to thermoelasticity. J Thermal Stress 1983;6(1):35–43.
[19] Cannarozzi AA, Ubertini F. A mixed variational method for linear coupled thermoelastic analyis. Int J Solids Struct 2001;38(4):717–39.
[20] Cho M, Oh J. Higher order zig-zag theory for fully coupled thermo-electric-mechanical smart composite plates. Int J Solids Struct 2004;41(5-6):1331–56.
[21] Carrera E. Historical review of zig-zag theories for multilayered plates and shells. Appl Mech Rev 2003;56(3):287–308.
[22] Oh J, Cho M. A finite element based on cubic zig-zag plate theory for the prediction of thermo-electric-mechanical behaviors. Int J Solids Struct 2004;41(5-6):1357–75.
[23] Ibrahimbegovic A, Colliat JB, Davenne L. Thermomechanical coupling in folded plates and non-smooth shells. Comput Methods Appl Mech Eng 2005;194(21-24):2686–707.
[24] Lee Z-Y. Generalized coupled transient thermoelastic problem of multilayered hollow cylinder with hybrid boundary conditions. Int Commun Heat Mass Transfer 2006;33(4):518–28.
[25] Tanaka M, Matsumoto T, Moradi M. Application of boundary element method to 3-D problems of coupled thermoelasticity. Eng Anal Bound Elem 1995;16(4):297–303.
[26] Carrera E, Boscolo M, Robaldo A. Hierarchic multilayered plate elements for coupled multifield problems of piezoelectric adaptice structures: formulation and numerical assessment. Arch Comput Methods Eng 2007;14(4):383–430.
[27] Daneshjoo K, Ramezani M. Coupled thermoelasticity in laminated composite plates based on Green-Lindsay model. Compos Struct 2002;55(4):387–92.
[28] Daneshjoo K, Ramezani M. Classical coupled thermoelasticity in laminated composite plates based on third-order shear deformation theory. Compos Struct 2004;64(3-4):369–75.
[29] Yang Q, Stainer L, Ortiz M. A variational formulation of the coupled thermo-mechanical boundary-value problem for general dissipative solids. J Mech Phys Solids 2006;54:401–24.
[30] Adam L, Ponthot J-P. Thermomechanical modeling of metals at finite strains: first and mixed order finite elements. Int J Solids Struct 2005;42(21-22):5615–55.
[31] Altay GA, Dökmeci MC. Coupled thermoelastic shell equations with second sound for high-frequency vibrations of temperature-dependent materials. Int J Solids Struct 2001;38(16):2737–68.
[32] Givoli D, Rand O. Dynamic thermoelastic coupling effects in a rod. AIAA J 1994;33(4):776–8.
[33] Wilms EV, Cohen H. Some one-dimensional problems in coupled thermoelasticity. Mech Res Commun 1985;12(1):41–7.
[34] Wauer J. On magneto-thermo-elastic vibrations. J Thermal Stress 1996;19(7):671–91.
[35] Kosinski W, Frischmuth K. Thermomechanical coupled waves in a nonlinear medium. Wave Motion 2001;34(1):131–41.
[36] Trajkoviski D, Cukic R. A coupled problem of thermoelastic vibrations of a circular plate with exact boundary conditions. Mech Res Commun 1999;26(2):217–24.
[37] Yeh Y-L. The effect of thermo-mechanical coupling for a simply supported orthotropic rectangular plate on non-linear dynamics. Thin-Walled Struct 2005;43(8):1277–95.
[38] Carrera E. A class of two-dimensional theories for multilayered plates analysis. Accademia delle Scienze Torino, Memorie Scienze Fisiche 1995:1–39.
[39] Carrera E. Theories and finite elements for multilayered plates and shells: a unified compact formulation with numerical assessments and benchmarking. Arch Comput Methods Eng 2003;10(3):215–96.
[40] Carrera E, Brischetto S. Vibrations of plates and shells in the case of thermo-mechanical coupling. In: The seventh international symposium on vibrations of continuous systems, Zakopane, Poland; July 19–25 2009.
[41] Reddy JN. Mechanics of laminated composite plates and shells. Theory and analysis. New York (USA): CRC Press; 2004.
[42] Mindlin RD. Influence of rotatory inertia and shear in flexural motions of isotropic elastic plates. J Appl Mech 1951;18:31–8.
[43] Cauchy AL. Sur l'équilibre et le mouvement d'une plaque solide. Exercise des Mathématique 1828;3:381–412.
[44] Poisson SD. Mémoire sur l'équilibre et le mouvement des corps élastique. Mémoires de l'Académie des Sciences des Paris 1829;8:357–570.
[45] Kirchhoff G. Über das gleichgewicht und die bewegung einer elastishen scheibe. Journal fur die reine und Angewandte Math 1850;40:51–88.
[46] Carrera E, Brischetto S. Analysis of thickness locking in classical, refined and mixed multilayered plate theories. Compos Struct 2008;82(4):549–62.
[47] Carrera E, Brischetto S. Analysis of thickness locking in classical, refined and mixed theories for layered shells. Compos Struct 2008;85(1):83–90.
[48] Leissa AW. Vibration of plates, NASA SP-160, Washington (DC, USA); 1969.

[49] Carrera E, Brischetto S, Nali P. Variational statements and computational models for multifield problems and multilayered structures. Mech Adv Mater Struct 2008;15(3):182–98.
[50] Ikeda T. Fundamentals of piezoelectricity. Oxford (UK): Oxford University Press; 1990.
[51] Spiessberger C, Gleiter A, Busse G. Aerospace applications of lockin-thermography with optical, ultrasonic and inductive excitation. In: International symposium on NDT in aerospace, Fürth, Germany; December 3–5 2008.
[52] Fantoni G, Merletti LG, Salerno A. Stato dell'arte della termografia lock-in applicata a componenti di elicottero: analisi termoelastica e rilevazione di difetti. Il Giornale delle Prove non Distruttive, Monitoraggio, Diagnostica 2008;4:30–4.
[53] Ibarra-Castanedo C, Grinzato E, Marinetti S, Bison P, Avdelidis N, Grenier M, et al. Quantitative assessment of aerospace materials by active thermography techniques. In: 9th International conference on quantitative infrared thermography, Krakow, Poland; July 2–5 2008.